Targeting Cell-Matrix Interface Mechanobiology by Integrating AFM with	<b>Fluorescence</b>
Microscopy	

Elizabeth R. Kahle <sup>a</sup> , Neil Patel <sup>a</sup> , Harini B. Sreenivasappa <sup>b</sup> , Michele S. Marcolongo <sup>c</sup> , Lin Han <sup>a,*</sup>
<sup>a</sup> School of Biomedical Engineering, Science, and Health Systems, Drexel University, Philadelphia, PA 19104, United States
<sup>b</sup> Cell Imaging Center, Office of Research and Innovation, Drexel University, PA 19104, United States
<sup>c</sup> Department of Mechanical Engineering, Villanova University, Villanova, PA 19085, United States

\*Correspondence and requests for materials should be addressed to:

Dr. Lin Han

Phone: (215)571-3821,

Fax: (215)895-4983,

Email: <a href="mailto:lh535@drexel.edu">lh535@drexel.edu</a>.

#### Abstract

Mechanosensing at the interface of a cell and its surrounding microenvironment is an essential driving force of physiological processes. Understanding molecular activities at the cell-matrix interface has the potential to provide novel targets for improving tissue regeneration and early disease intervention. In the past few decades, the advancement of atomic force microscopy (AFM) has offered a unique platform for probing mechanobiology at this crucial microdomain. In this review, we describe key advances under this topic through the use of an integrated system of AFM (as a biomechanical testing tool) with complementary immunofluorescence (IF) imaging (as an in situ navigation system). We first describe the body of work investigating the micromechanics of the pericellular matrix (PCM), the immediate cell micro-niche, in healthy, diseased, and genetically modified tissues, with a focus on articular cartilage. We then summarize the key findings in understanding cellular biomechanics and mechanotransduction, in which, molecular mechanisms governing transmembrane ion channel-mediated mechanosensing, cytoskeleton remodeling, and nucleus remodeling have been studied in various cell and tissue types. Lastly, we provide an overview of major technical advances that have enabled more in-depth studies of mechanobiology, including the integration of AFM with a side-view microscope, multiple optomicroscopy, a fluorescence recovery after photobleaching (FRAP) module, and a tensile stretching device. The innovations described here have contributed greatly to advancing the fundamental knowledge of extracellular matrix biomechanics and cell mechanobiology for improved understanding, detection, and intervention of various diseases.

### **Keywords**

Atomic force microscopy, nanomechanics, mechanotransduction, pericellular matrix, cytoskeleton, ion channels.

#### 1. Introduction

Since its invention in the 1980s (Binnig et al., 1986), atomic force microscopy (AFM) has witnessed exponential growth in applications across multiple disciplines, spanning materials science, physics, chemistry, biology and medical science. While originally purposed as a surface characterization tool, AFM has emerged as a common modality for small-scale mechanical measurements. In biomedical research, owing to its ease of operation in fluids, versatility in force ranges and contact geometries, AFM is now a standard tool for quantifying the micro- and nanomechanics of biological tissues, cells and biomacromolecules (Ando et al., 2013; Han et al., 2017; Li et al., 2017). This technique has been used in multiple loading modes, such as a nanotribometer to measure frictional and shear properties of bio-interfaces and tissue surfaces (Coles et al., 2008; Han et al., 2007a; Han et al., 2007b), or a molecular force sensor to quantify intra- and intermolecular interactions (Abu-Lail et al., 2006; Dean et al., 2006; Han et al., 2008; Oberhauser et al., 1998; Rief et al., 1997; Rojas et al., 2014), or has been customized into a nanorheometer to assess time-dependent poroviscoelastic properties (Azadi et al., 2016; Connizzo and Grodzinsky, 2018; Han et al., 2011a; Nia et al., 2013). Among these many applications, the most common one is for AFM to serve as a nanoindenter for quantifying the elastic and viscoelastic indentation properties of biological samples. For uncalcified biological samples, AFM-based nanoindentation has several advantages over instrumented nanoindentation, as it is suitable for quantifying material moduli spanning ten orders of magnitude (from ~ 1Pa to 10 GPa), and is much less time consuming with regards to sample preparation and quantification of µm-scale spatial heterogeneity (Han et al., 2017). As early as the 1990's, AFM has been used to quantify cell biomechanics (A-Hassan et al., 1998; Barbee et al., 1995). Since then, in alignment with the progression of experimental characterization methods, a comprehensive theoretical framework has been established for extracting elastic and time-dependent poroviscoelastic properties from the nanoindentation outcomes (Lin and Horkay, 2008; Mattice et al., 2006). Even for calcified tissues, AFM nanoindentation has demonstrated its unique applications in studying nanoscale anisotropy and heterogeneity (Tai et al., 2007), and the recently available commercial PeakForce nanomechanical mapping module has demonstrated its potential in delineating nanoscale heterogeneity beyond the resolution of conventional instrumented nanoindentation (Rux et al., 2022; Zhou et al., 2020b).

Given its high sensitivity in force and spatial resolution, AFM has become a major tool in understanding the mechanobiology at cell-matrix interfaces (Krieg et al., 2019; Sen and Kumar, 2010). Interactions at cell-matrix interfaces are a crucial driving force of cell signaling, homeostasis, matrix integrity as well as disease pathogenesis (Humphrey et al., 2014) (Fig. 1). On the matrix front, in many tissue types, the immediate microniche of cells is distinct from the bulk of the ECM. Cells are often surrounded by a complex pericellular coating consisting of proteoglycans, glycosylated lipids and transmembrane glycoproteins, termed as the "glycocalyx layer". The glycocalyx layer plays crucial roles in regulating cell plasma membrane architecture, integrin-matrix interactions, and other mechanosensitive signaling (Kuo and Paszek, 2021). In studies on tumor metastasis, the bulky glycocalyx layer of cancer cells has been shown to facilitate integrin clustering by funneling active integrins into adhesion sites and altering integrin state by applying tension to matrix-bound integrins arising from its fixed charges in a manner independent of actomyosin contractility, a mechanism termed as "kinetic trap". In circulating tumor cells, the abundantly expressed glycoproteins are suggested to promote focal adhesion assembly as well as integrin-dependent signaling, cell growth and survival, underlying the importance of glycocalyx layer in the metastatic cell phenotype (Paszek et al., 2014).

In tissues with dense matrices, the pericellular layer is further defined by a hierarchically assembled, mechanically functional micro-domain that has distinct composition and structure relative to bulk matrix, known as the "pericellular matrix" (PCM) (Wilusz et al., 2014). The PCM shows exclusive localization or preferential localization of glycoproteins, proteoglycans and proteoglycan-hyaluronan complexes (Möckl, 2020; Wilusz et al., 2014), as well as thinner collagen fibrils (Chery et al., 2021). The PCM is also where initial events of matrix assembly, including collagen fibrillogenesis and proteoglycan-hyaluronan association take place (Birk and Brückner, 2011; Quinn et al., 1999). Given its immediate contact with cells, the PCM plays a pivotal role in regulating cell mechanosensing such as cell-matrix adhesion, migration, solute transport, growth factor sequestration, stem cell fate, metastasis, and is often the site of disease initiation (Ferreira et al., 2018; Guilak et al., 2018).

On the cell front, interactions between cells and their microenvironment are essential for physiological processes such as signaling, development, and homeostasis (Humphrey et al., 2014). Cells sense their environment through mechanosensitive molecules at the cell membrane, such as integrins, stretch-activated ion channels, G protein coupled-receptors, and growth factor receptors (Martino et al., 2018). Specifically, integrin-mediated cell adhesion is a major mechanism of cell mechanotransduction. In vivo, integrins bind to ECM molecules such as collagens and fibronectin. This binding enables the formation of focal adhesion sites, activating a cascade of intracellular events, including F-actin polymerization, activation of the RhoA-ROCK (Rho-associated protein kinase) pathway and mechano-adapation of LINC (Linker of Nucleus and Cytoskeleton) complex on the nucleus membrane (Heo et al., 2018; Li et al., 2016; Sun et al., 2016) (Fig. 1). These events modulate the conformation of chromatin in the nucleus, as well as downstream cell signaling and functions. In turn, the type and amount of specific integrin expressions are also driven by the composition and structure of ECM, contributing to the feedback loop of cell-matrix interactions (Seetharaman and Etienne-Manneville, 2018). Indeed, ECM and cell-generated force propagation is ensured by the regulation of cytoskeletal tension, modulated by stress fibers (SF) comprised of motor protein myosin II, F-actin, and cross-linking proteins. Alterations in second messengers, such as cytoskeletal tension, distribute the external stimuli signals to a wide variety of intracellular enzymes and ion channels (Martino et al., 2018). Ion channels, including transient receptor potential vanilloid-type 4 (TRPV4), Piezo1/2, and voltage-gated calcium channels (VGCC), are activated upon external stimuli via second messengers, and mediate the mechano-responses of cell development and disease initiation (Jin et al., 2020; Martinac, 2004). Changes in nuclear and cytoskeletal organization, as well as ion channel activities, are direct manifestations of cell phenotypic shifts in response to mechanosensing of the microenvironment. For both the cell and matrix, fluorescence microscopy is commonly used for quantifying the composition and distribution of ECM/PCM molecules, as well as the structure of subcellular organelles. To this end, synergistic application of AFM as a mechanical tool, and fluorescence microscopy as a complementary real-time imaging modality, enables a unique platform for probing micromechanobiology at the cell-matrix interface.

This review focuses on the synergistic applications of AFM and fluorescence microscopy throughout the studies of mechanotransduction, in which, AFM was used as a nanomechanical testing tool with complementary fluorescence imaging as an *in situ* navigation system. The general applications of AFM in the characterization of the structure (Cascione et al., 2017; Jung et al., 2010), biomechanics, and mechanobiology (Kiio and Park, 2020; Liang et al., 2020; Ozkan et al., 2016) of cells and ECM can be found in a few recent review articles. Thus, this

review focuses on the axis of cell-matrix interface interactions, including the PCM, transmembrane ion channels, cytoskeleton, and nucleus. Section 2 describes the body of work on matrix biomechanics by total internal reflectance fluorescence microscopy (TIRF)-guided AFM nanomechanical mapping, with an emphasis on its applications in the PCM. These studies have been primarily focused on musculoskeletal tissues, and in particular, articular cartilage. whose PCM has been studied most extensively (Guilak et al., 2018; Wilusz et al., 2014). Section 3 summarizes the key findings in the biomechanics and mechanobiology of cells as well as nuclear mechanics. AFM and fluorescence imaging have been applied simultaneously to quantify single cell biomechanics and subcellular structure to find correlations between the two. Meanwhile, AFM has also been used as a force transducer to apply forces to cells or subcellular constituents, while fluorescence imaging was used to measure the structural or signaling outcomes. These applications were conducted in a wider spectrum of musculoskeletal, cardiovascular, immunoengineering, and cancer research. Section 4 presents technical advances on this front, in which, customized modifications were applied to further expand the applications of AFM-based nanomechanical testing and fluorescence imaging. In the closing section 5, we provide our remarks on challenges and future opportunities of these technologies.

## 2. Applications in Pericellular Matrix Biomechanics

For the past decade, AFM-nanomechanical mapping has been applied with fluorescence imaging to delineate the micromechanics of PCM versus bulk ECM on tissue cryo-sections (Wilusz et al., 2012b). To this day, although the PCM is a prominent feature in many tissue types, TIRF-guided AFM has mainly been applied to articular cartilage, except for one study on the meniscus (Sanchez-Adams et al., 2013). This section focuses the applications of AFM and fluorescence imaging in the understanding of PCM biomechanics in healthy, degrading, and regenerative cartilage tissues.

#### 2.1. Micromechanics of PCM in healthy and diseased tissues

In the pioneering work by Darling et al., AFM force-volume mapping was first applied to the cryo-sections of human, porcine, and murine cartilage samples to demonstrate the feasibility of assessing tissue microscale heterogeneity (Darling et al., 2010). Building on this work, Wilusz et al. integrated AFM with real-time TIRF imaging, in which, IF-labeling of the PCM biomarker, collagen VI, was used to separate the micromodulus of PCM and bulk ECM (territorial/interterritorial matrix, or T/IT-ECM) via image registration (Fig. 2a). The use of a microspherical tip provides sufficient resolution to delineate the micromoduli of the matrix from those representing the cell remnants, and to quantify the spatial heterogeneity of PCM and T/IT-ECM (Wilusz et al., 2012b). For example, with an indenter with  $R \approx 2.5 \, \mu \text{m}$  radius, a maximum indentation depth ≈ 100 nm yields ≈ 0.7 µm tip-sample contact radius. Given that the stress fields are largely constrained to the region directly underneath the tip-sample contact area within the Hertzian contact framework (Johnson, 1985; Jacobs et al., 2010), this method yields a spatial resolution at the sub-um level. With this method, the anisotropy and heterogeneity of PCM was quantified in healthy porcine cartilage. The PCM exhibited uniform mechanical properties from superficial to deep zones, unlike the case of bulk ECM. On the other hand, similar to that of bulk ECM, PCM exhibited apparent anisotropy throughout tissue depth (McLeod et al., 2013). Also, the PCM was found to be resistant to broader enzymes that are known to degrade cartilage bulk ECM, including chondroitinase ABC and hyaluronidase (Wilusz

and Guilak, 2014), further underscoring the distinctiveness of this microdomain. In contrast to this uniformity in cartilage, appreciable zonal variation of PCM was detected in porcine meniscus, in which, the tension-bearing fibrous outer region had higher modulus in both the PCM and bulk ECM than the compression-bearing inner region (Sanchez-Adams et al., 2013).

Given its immediate contact with chondrocytes, the PCM is highly sensitive to altered metabolism during the initiation of osteoarthritis (OA). In cartilage specimens from early OA patients, both the PCM and bulk ECM showed significant reduction in micromodulus. This reduction was accompanied by the radial expansion of PCM labelled by collagen VI (Wilusz et al., 2013), illustrating the loss of both structural and mechanical integrity of PCM (Fig. 2b). Such observation also corroborated a more recent study showing the progressive reduction of PCM micromodulus with increased cell clustering (Danalache et al., 2019). Together, these results suggest that early OA is marked by micromechanical damage of PCM and associated aberrant cell proliferation.

While studying human specimens provides direct clinical relevance, testing animal models enables a mechanistic understanding of disease pathogenesis. In murine OA model, the PCM was identified as one leading site of disease initiation and possibly a casual factor of more widespread matrix degeneration. Following the destabilization of the medial meniscus (DMM) surgery (Chery et al., 2020), a prevalent in vivo post-traumatic OA model (Glasson et al., 2007), the reduction of PCM micromodulus in wild-type (WT) mice was apparent as early as 3 days post-surgery, which precedes changes in both the bulk ECM properties 1 week after (Doyran et al., 2017), and overt histological indications of cartilage damage 4-8 weeks after DMM (Glasson et al., 2007) (Fig. 2c). This early degeneration can be attributed to the degradation of aggrecan, the major cartilage proteoglycan, as its degradation neo-epitopes are localized in the PCM at this early stage (Singer et al., 1995). The degeneration of PCM was also associated with demoted chondrocyte calcium signaling activities, [Ca<sup>2+</sup>]<sub>i</sub>, one of the earliest and most fundamental cell responses to biomechanical cues (Clapham, 2007). In turn, when PCM degeneration was partially blocked by the small molecule MMP-inhibitor, GM6001, both the PCM micromechanics and chondrocyte calcium signaling were restored toward the baseline level (Chery et al., 2020).

Therefore, aided by AFM testing and IF imaging, changes at the cell-matrix interface were identified as an early hallmark of wide-spread, progressive tissue degeneration. The PCM could potentially serve as a new target for OA detection and initiation. This concept, while established on cartilage, could be applicable to other load-bearing and mechanosensitive tissues as well. On the technical front, application of IF-AFM to murine tissue sections was limited by its small size and integration with the bony tissue. Such technical challenges could be overcome by applying Kawamoto's film-assisted cryo-sectioning (Kawamoto and Kawamoto, 2014), which prevents the fracturing of underlying bony tissues and maintains soft tissue integrity during cryo-sectioning. It is worth noting that it is unclear how the properties of PCM in cartilage and other tissues vary across different joint types (e.g., ankle, knee, hip, TMJ) and species. Such knowledge gaps, addressable by the IF-AFM technique, could provide a foundation to translate findings from animal models to clinical applications of OA and other mechanosensitive diseases.

#### 2.2. Roles of individual matrix molecules in PCM biomechanics

Given the distinct molecular composition of the PCM, several studies have aimed at pinpointing the roles of individual matrix molecules in the integrity and mechanobiological functions of the

PCM. Biomechanical significance of the two major cartilage PCM biomarkers, collagen VI and perlecan, was investigated. In cartilage, perlecan, a heparan sulfate (HS) proteoglycan, regulates cell mechanosensing and activation of fibroblast growth factor-2 (FGF-2) (Vincent et al., 2007), and stabilizes PCM through interactions with collagens VI and XI (Guilak et al., 2021). The contribution of perlecan heparan sulfate-glycosaminoglycan (HS-GAG) chain to PCM biomechanics was assessed by evaluating the impact of heparinase III digestion on porcine cartilage cryo-sections (Wilusz et al., 2012a). The digestion increased the PCM micromodulus, and thus, it is hypothesized that perlecan and its HS-GAGs soften the PCM by shielding the stiffer fibrillar constituents, contributing to the native cellular microenvironment for proper cell mechanotransduction.

Additionally, genetic ablation of collagen VI was found to impair the PCM integrity. In *Col6a1*<sup>-/-</sup> mice, the PCM exhibited reduced modulus relative to age-matched WT controls at both young adult (2 months) and mature (9 months) ages (Zelenski et al., 2015) (Fig. 3a). This softening of PCM was in alignment with increased chondrocyte swelling and TRPV4-mediated [Ca<sup>2+</sup>]<sub>i</sub> signaling in response to hypo-osmotic stimuli *in situ*, illustrating the role of collagen VI in mediating the PCM integrity and chondrocyte mechanosensing. Interestingly, despite the impairment of PCM, the bulk ECM of *Col6a1*<sup>-/-</sup> cartilage did not show an appreciable phenotype. Meanwhile, loss of collagen VI led to accelerated hip OA (Alexopoulos et al., 2009), but attenuated knee OA (Christensen et al., 2012) in aged *Col6a1*<sup>-/-</sup> mice, indicating that the role of collagen VI in cartilage health may vary with disease stage and location.

Our recent studies highlighted the crucial role of decorin, a small leucine-rich proteoglycan (SLRP), in the mechanobiological functions of PCM. In cartilage, decorin is present throughout the ECM, but is more concentrated in the PCM. At the whole tissue-level, decorin strengthens the assembly of the aggrecan network in the ECM, and thus, is essential for both maintaining tissue-level biomechanical properties of cartilage (Han et al., 2019) and slowing the degeneration of cartilage in OA (Han et al., 2021; Li et al., 2020). At the microscale, loss of decorin was found to reduce aggrecan content and micromechanics of the PCM, and this effect became progressively more pronounced from newborn (3 days) to adult (3 months) ages in  $Dcn^{-/-}$  mice, as assessed by IF-AFM (Chery et al., 2021) (Fig. 3b). In turn, loss of decorin resulted in demoted [Ca<sup>2+</sup>]<sub>i</sub> activities in situ, which was attributed to the reduction of fixed negative charges in the immediate cellular microenvironment. Thus, despite not being a PCM-exclusive molecule, decorin also plays a crucial role in regulating the biomechanics and mechanobiological functions of cartilage PCM by mediating the assembly and retention of aggrecan therein.

A few other molecules were also studied in the context of PCM integrity. Collagen III is a minor fibril-forming collagen that is present in cartilage at low concentration (~ 1-5%) and is more concentrated in the PCM (Hosseininia et al., 2016). Reduction of collagen III was also found to impair the micromodulus of cartilage PCM in *Col3a1*+/- mice, which could be due to the impaired assembly of collagen II fibrils, rather than reduction of proteoglycans (Wang et al., 2020). Collagen V is a regulatory fibril-forming collagen that primarily mediates the initial assembly of collagen I fibrils (Birk and Brückner, 2011). Impact of collagen V on cartilage PCM was studied in the context of temporomandibular joint (TMJ) cartilage, a hybrid tissue of collagen I-dominated fibrocartilage and collagen II-rich hyaline cartilage. Reduction of collagen V was found to impair the micromodulus of PCM in the hyaline layer in the TMJ condyle of *Col5a1*+/- mice. This was attributed to the altered proliferation and chondrogenesis of progenitor cells with

the loss of collagen V in the fibrous layer, and thus, impaired matrix development (Chandrasekaran et al., 2021). Besides the aforementioned matrix molecules, there are many other constituents that are either exclusively or preferentially distributed in the PCM, such as collagens IX, XI, matrilins, chondroadherin and cartilage oligometric matrix protein (COMP) (Batista et al., 2014; Han et al., 2011b; Heinegård, 2009; Heinegård and Saxne, 2011). Applying IF-AFM to genetic murine models of these molecules could shed new insights into the mechanobiological functions of cartilage PCM, and thus, help identify new targets for disease intervention or regeneration.

### 2.3. Engineering of PCM biomechanics

One key characteristic of cartilage PCM is the high fixed charge density endowed by the residing proteoglycans, especially aggrecan. In disease, degeneration of aggrecan leads to loss of local fixed charge density, contributing to disrupted chondrocyte mechanotransduction (Chery et al., 2020). As such, an array of biomimetic proteoglycans (BPGs) were developed to partially imitate the molecular architecture and biophysics of aggrecan and other proteoglycans (Prudnikova et al., 2018; Prudnikova et al., 2017). For instance, BPG10, a "bottle-brush"-like synthetic polymer comprised of ~6-7 CS-GAGs conjugated onto a ~10 kDa poly(acrylic acid) (PAA) core, has demonstrated the potential to molecularly engineer cartilage mechanotransduction through modulation of the existing cellular microniche of the PCM. Upon diffusion into bovine cartilage explants, BPG10 was found to be localized in the PCM and surrounding territorial domains, possibly due to its molecular adhesion with native aggrecan molecules. Such localization was found to augment the PCM micromodulus (Fig. 3c). As a result, chondrocyte [Ca<sup>2+</sup>]; signaling was also enhanced under both physiologic and osmoticallystimulated environment. It was thus suggested that BPG10, and perhaps other BPGs, could serve as a potential molecular therapy by targeted engineering of PCM biomechanics and cell-PCM mechanosensing (Kahle et al., 2022).

In addition to explant studies, IF-AFM was also implemented to assess the newly deposited PCM by chondrocytes in vitro to gain new insights into cell-matrix interactions for improved design of hydrogels in tissue engineering. Bovine chondrocytes were cultured in both soft (~ 5 kPa) and stiff (~ 20 kPa) hyaluronan-based hydrogels, and the newly synthesized proteins and GAGs were labeled by the functional noncanonical amino acid tagging (FUNCAT) method via click chemistry (Loebel et al., 2019; McLeod and Mauck, 2016). Despite being surrounded by a much stiffer native PCM in vivo (~ 50 kPa in human (Wilusz et al., 2013), ~ 60 kPa in bovine (Kahle et al., 2022), and ~ 1 MPa in mice (Chery et al., 2021)), when chondrocytes are cultured in vitro, much softer hydrogels (~10-20 kPa) are required to maintain cell viability and prevent dedifferentiation (Wang et al., 2016). In engineered hydrogel systems, deposition of nascent proteins and GAGs were apparent as early as one day after culture. These nascent molecules were more confined near the cell surface in the stiffer hydrogel than in the softer one. At 7 days of culture, the micromodulus of the neo-PCM was similar (~ 15 kPa) in both hydrogels at the vicinity of cells and underwent progressive change toward the hydrogel bulk modulus radially. Thus, it was suggested that the distribution and assembly of nascent matrix was influenced by the existing microenvironment. On the other hand, cells also demonstrated self-adaptivity to the microenvironment, as the local modulus of immediate cell-matrix interface was similar (~ 15 kPa) despite differences in the bulk hydrogel properties (Loebel et al., 2020).

## 3. Applications in Cell Biomechanics and Mechanobiology

One major contribution of synergistic AFM and IF imaging was in uncovering the molecular activities governing cell mechanotransduction. These studies have investigated the dynamic changes in cytoskeletal and nuclear structure, as well as cell mechanical properties to elucidate the structure-mechanics relationships at the sub-cellular scale. AFM has also been used as a force transducer to induce mechanical stimuli, which allows for real-time tracking of subcellular structural changes or intracellular calcium activities under fluorescence microscopes to elucidate the roles of molecular constituents in cell mechanosensing. This section describes the mechanobiology knowledge generated on the transmembrane ion channel, cytoskeleton, and nucleus in various cell and tissue types.

#### 3.1. Mechanotransduction of transmembrane ion channels

The transmembrane ion channels play a key role in mediating cell sensing of their immediate microenvironment. The pioneering work by Charras et al., demonstrated the feasibility of monitoring cell calcium influx under mechanical stimulation by AFM tips (Charras and Horton, 2002; Charras et al., 2001). In this study, osteoblasts isolated from neonatal rats were labelled with Fluo3-AM for intracellular calcium imaging and subjected to AFM-nanoindentation and force relaxation using colloidal microspherical tips. During indentation, deformation of the cell membrane and spontaneous calcium influxes were recorded via confocal imaging simultaneously. This set-up enabled direct observation of the activation of strain-induced intracellular calcium signaling, as well as the transmission of calcium influxes to adjacent cells. Results identified two cellular responsive pathways to mechanical stimuli, in which the ion channels were responsible for the fast activation due to stretching of the cell membrane, followed by a longer relaxation phase mediated by the cytoskeleton. Interestingly, through selective disruption of cytoskeletal constituents, this study identified microtubules and vimentin, but not F-actin, as moieties required to modulate this longer relaxation phase.

In addition to osteoblasts, similar approaches were applied to other cell types, including myoblasts and immune cells. Formigli et al., used commercial pyramidal AFM tips to stretch C2C12 myoblasts through tip-cell adhesion during cantilever retraction and noted an increase in calcium influx, which also propagated to adjacent cells through cell-cell contact gap junctions (Formigli et al., 2005). Similarly, Cazaux et al., stimulated T cells and macrophages with a rampand-hold force relaxation using microspherical tips and recorded simultaneous calcium pulses. Meanwhile, they applied controlled photo-activation of Rac, a small G protein, in T cells and quantified the simultaneous mechanical changes via AFM (Cazaux et al., 2016). These studies have demonstrated a broad potential for studying ion channel-mediated mechanotransduction in multiple cell types and diseases by integrating AFM and immunofluorescence imaging.

Lee et al., uncovered the pivotal roles of Piezo1/2 ion channels in the mechanotransduction and immune responses of chondrocytes (Lee et al., 2014; Lee et al., 2021). A tipless AFM cantilever was used to compress individual cells up to the strain mimicking injurious loading (~ 50%), and the resulting calcium influx was recorded simultaneously via an inverted bottom-up fluorescence microscope. The key role of Piezo1/2 ion channels were evidenced by the pronounced Ca<sup>2+</sup> influx of Piezo1/2-co-transfected neuro2A cells, which had no response to mechanical stimulation without transfection. Conversely, in chondrocytes, knockdown of Piezo1/2 via siRNA or small molecule Piezo inhibitor, GsMTx4, led to substantial reduction of mechanically evoked Ca<sup>2+</sup>-influx (Fig. 4a). In turn, inhibition of Piezo1/2 channels was shown to reduce chondrocyte

death under injurious loading (Lee et al., 2014). Their recent follow-up study further elucidated the role of Piezo1 in the mechanoresponses of chondrocytes under inflammatory stimulation. A tipless cantilever was used to induce cyclic compressive loading to chondrocytes, and the resultant intracellular calcium content and flux were monitored. Outcomes showed increased responses in mechanically evoked  $[Ca^{2+}]_i$  activities under the stimulation of inflammatory cytokine interleukin (IL)-1 $\alpha$ . This increase in  $Ca^{2+}$  influxes was attenuated by 2  $\mu$ M GsMTx4 + 5  $\mu$ M dynasore that inhibit the Piezo channels, but not by GSK205 or verapamil, inhibitors of TRPV4 and VGCC, respectively (Fig. 4b). Such response was found to be mediated by inflammation-induced upregulation of the IL1R-p38 MAP-kinase pathway, which up-regulates Piezo1. Increased Piezo1 function led to rarefication of F-actin, which was suggested to contribute to the stiffness reduction and phenotypic shift of chondrocytes in OA (Lee et al., 2021). It was thus hypothesized that inhibition of Piezo1 channel could play a protective role in reducing mechanical injury-induced cartilage damage and OA progression.

### 3.2. Mechanotransduction and remodeling of cytoskeleton

Dynamics of actin filaments are a major driving force of cell mechanotransduction. Earlier studies have applied AFM to induce mechanical perturbations to the apical surface of bovine aortic endothelial cells, and the time-dependent distal displacement was monitored in 3D by tracking integrin-bound fluorescent nanoparticles via defocused microscopy (Rosenbluth et al., 2008). Outcomes identified a distance-dependent slow stress propagation in response to external mechanical stimuli, which was explained by the poroelastic model to account for both actin-mediated cytoskeletal deformation and flow of cytoplasm. Also, AFM force curve-based topographical imaging was coupled with fluorescence imaging to observe the dynamic changes in the cortical actin network in live vascular endothelium cells, and confocal microscopy was applied to directly observe the actin-destabilization (Kronlage et al., 2015). AFM nanoindentation and bottom-up fluorescence imaging were performed simultaneously on GFP-transfected NIH 3T3 fibroblasts (Gavara and Chadwick, 2016). Results showed that the amount of myosin, and to a lesser extent, actin assembled in the stress fibers are major determinants of cell stiffness.

In cancer-related research, AFM-nanoindentation was applied with spinning disk confocal microscopy (SDCM) to directly observe the local deformation of the cell membrane and cytoskeleton during nanoindentation. Comparing cells with (NIH 3T3 fibroblasts) or without (MDA-MB-231 breast cancer cells) the perinuclear actin cap (apical stress fibers), it was highlighted that the actin cap is a major determinant of the higher stiffness and mechanical anisotropy observed in 3T3 fibroblasts (Efremov et al., 2019). Also, AFM nanoindentation, confocal microscopy and a bi-layered finite element modeling were applied to decouple the modulus of MDA-MB-231 cells with their surrounding 3D environment in collagen I-based hydrogels. A positive correlation was found between the stiffness and invasiveness of cells into a collagen hydrogel, and actomyosin contractility was identified as one major mechanism of the initial metastatic invasion (Staunton et al., 2016).

Two key studies elucidated the growth and deformation mechanisms of actin networks at the molecular level. Parkesh et al. studied the dynamics of Arp2/3 complex-activated actin network formation between two flat nucleating surfaces of an ActaA-coated tipless cantilever and substrate. Growth of the actin network was measured by the deflection of the actin-associated cantilever up to ~100 nN force, while epifluorescence images were taken to quantify the size of the polymerized actin network during growth. In doing so, they demonstrated the load-

dependent growth of the actin network, and showed that the force-growth velocity relationship of the actin network was dependent on the loading history (Parekh et al., 2005) (Fig. 5a). Using this setup, Chaudhuri et al. further elucidated the reversible stress softening mechanism of dendritic actin networks, where the AFM cantilever served as both a nucleating surface and a microrheological device (Chaudhuri et al., 2007). In response to a sinusoidal load at 0.1-20 Hz, actin networks exhibited stress-stiffening up to the critical stress ~ 233 Pa, followed by reversible softening at higher stresses (Fig. 5b). This behavior was attributed to entropic elasticity as filaments are extended, leading to a stress-stiffening regime and reversible buckling of actin filaments at higher loads. This non-linear mechanics of actin networks was also noted at the cellular level. When fibronectin-coated AFM spherical tips were used to apply cyclic tension to fibroblasts from rat vomeronasal organs, an initial increase in tension was followed by a decrease due to stress relaxation of the actin network followed by a long-term, slow increase in tension as the cycles persisted, likely due to the diffusion limited recruitment of myosin II (Watanabe-Nakayama et al., 2011). This response was suggested to contribute to the adaptive, and possibly self-protective mechanoresponse of cells, where they initially stiffen under the stimulation of an external force, but then, become increasingly insensitive to repeated perturbations.

In addition to actin filaments, microtubules also contribute to the time-dependent cell mechanics. When 3T3 fibroblasts were perturbed by AFM, organelle displacement at locations far from the initial contact point could be detected. Such long-range displacement was suggested to be mediated by both actin and microtubule cytoskeletons (Silberberg et al., 2008). Similarly, when compressed by tipless AFM cantilevers, L929 fibroblasts exhibited locally distinct changes in shape and depth of cytoskeleton imprints due to force propagation through the cytoskeleton, as observed by TIRF imaging of basal membrane topography. Upon disruption of each cytoskeleton constituent, it was shown that both actin filaments and microtubules contribute to cell stiffness and force transduction throughout the cytoplasm (Jonas and Duschl, 2010). Also, simultaneous volumetric images of lysosome trafficking, vimentin nuclear caging, and actin dynamics have been achieved on HeLa cells under AFM-nanoindentation via volumetric light sheet fluorescence microscope (LSFM), illustrating the feasibility to uncover the roles of vimentin, a representative intermediate filament cytoskeleton, in cell biomechanics and its stiffening effect under applied forces (Nelsen et al., 2020).

#### 3.3. Nuclear Mechanics and Mechanobiology

Nuclear mechanics, an emerging field within the study of cellular mechanics, has substantially benefited from the combination of AFM and fluorescence imaging. These techniques have revealed how interactions between cells and their surrounding environment can impact the behavior of the nucleus, as well as two primary determinants of nuclear biomechanics, chromatin and lamin A/C. Confocal microscopy has been applied to track nuclear deformation induced by AFM-nanoindentation to extract biomechanical properties of the nucleus (Krause et al., 2013). For example, mechanical anisotropy of the nucleus was demonstrated by tracking the 3T3 fibroblast nucleus deformation induced by pyramidal AFM tips via laser confocal scanning microscopy (LCSM) (Haase et al., 2016). A higher strain was observed along the minor axis of the elliptical-shaped nucleus. This anisotropy was found to be mediated by actin filaments along the minor axis and microtubules along the major axis. Inside the nucleus, balance between chromatin organization, an outward entropic force, and lamin A/C localization, a containment force, was shown to contribute to the inherent non-isotropic mechanical properties.

Beicker et al., built a vertical light sheet enhanced-side view fluorescence microscope integrated with AFM to monitor nuclear morphology during compression by microspherical indenters ( $R \approx 2.5 \, \mu m$ ) (Beicker et al., 2018). Two stiffness regimes were detected from the indentation response of ovarian cancer SKOV3 cells, where a  $1.5 \times$  increase in modulus was found at  $\approx 0.6 \, \mu m$  indentation depth. In tracking the positions and structures of cell/nuclear membrane and structures, they found that the first regime was due to cytoplasmic deformation and attributed the modulus increase to the onset of nucleus deformation. In a follow-up study, they decoupled the contributions of chromatin and lamin A/C to the non-linear mechanical properties (Hobson et al., 2020). Using nuclear cross-sectional area and perimeter as surrogates for nuclear volume and surface area, they correlated the indentation force with nuclear morphological changes. Assisted by an empirical numerical model of strain-stiffening effect, they showed that chromatin and lamin A/C are separately resisting changes in nuclear volume and surface area, respectively.

As the nucleus is wrapped inside the cytoplasm, direct quantification of nuclear biomechanics was made possible using AFM needle-tips (R < 200 nm) to penetrate through cell plasma and nuclear membranes. Sharp needle-like AFM tips were fabricated by focused ion beam (FIB) milling and applied to various cell types (Liu et al., 2014). During indentation, puncture of cell plasma and nuclear membranes, and subsequent deformation of chromatin, were visualized by laser confocal scanning microscopy, allowing the separation of cytoplasmic and nuclear moduli. A pronounced softening effect of nuclei was found once nucleus was isolated from fibroblast-like cells. Additionally, the more invasive T24 bladder carcinoma cell line showed softer nuclei than the non-invasive RT4 line, illustrating nuclear biomechanics as a possible indicator of metastatic potential. Recently, McCreery et al., applied the needle-tip technique to elucidate the dynamics of cell membrane repair and nucleus-ECM cross-talk (McCreery et al., 2021). HeLa cells were transfected with CHP4B-GFP, a protein required for the repair of damaged plasma and nuclear membranes, to monitor the active repair process following the needle-tip puncture. Confocal imaging enabled the correlation of plasma/nuclear membrane penetration with the local force peaks of each F-D curve and the validation of membrane repair by the intracellular intensity of CHP4B (Fig. 7a). Also, applying this set-up to vibratomed cryo-sections of bovine cartilage, they demonstrated significant softening of chondrocyte nuclei when the residing ECM was enzymatically degraded by MMP-13 or ADAMTS-4, highlighting the interconnectivity of nucleus. cytoskeleton, and the surrounding ECM.

Recent work by Raman and colleagues further quantified the nanomechanics of nucleolus, the non-membranous nuclear body consisting of highly compacted proteins and RNAs, by integrating the multi-harmonic, dynamic AFM with confocal imaging. In this mode, a soft cantilever (nominal k < 0.1 N/m) was excited by Lorentz force near its resonance frequency during the indentation on the cell surface. Maps of zeroth to second order harmonic amplitudes,  $A_0$ ,  $A_1$  and  $A_2$ , as well as phase angles,  $\phi_1$ ,  $\phi_2$ , were obtained in fluid. Storage and loss moduli were extracted by analyzing these terms in the Hertzian contact mechanics framework with corrections for near-surface hydrodynamics (Raman et al., 2011). This set-up was further tuned for cell nanomechanical mapping by the use of microfabricated tips with long-carbon tips to minimize the hydrodynamic squeeze film effects and achieve subcellular resolution, as well as the integration with spinning disk confocal microscopy to confirm the identity of intracellular structures, size, and locations in the cells (Efremov et al., 2022). Aided by live fluorescent markers of nucleoli and F-actin, the moduli of nucleoli in NIH 3T3 fibroblasts and MDA-MB-231 breast cancer cells were quantified (Fig. 6b). The nucleoli showed ~ 2× higher storage modulus

than surrounding areas for both cell types, which was attributed to the highly compacted conformation of residing proteins and RNAs. In comparison to 3T3 fibroblasts, MDA-MB-231 cells showed a larger size of their nucleoli, which was correlated with the high ribosome RNA synthesis, cell growth and metabolism in this cancer cell line. In contrast to other studies, for both cell types, the nucleus itself did not yield higher modulus relative to the surrounding cytoplasm and was suggested to have similar properties at this length scale.

## 4. Technical Advances in Customized AFM-Fluorescence Imaging Devices

Recent technical advances have enabled specialized and more in-depth characterization of cell mechanotransduction beyond the classical AFM-based nanomechanical testing coupled with IF imaging. This section presents four extended modes, including the implementation of side-view optical imaging, multiple optomicroscopy, fluorescence recovery after photobleaching (FRAP), and a tensile device integrated with AFM. We also summarize new findings from these modes.

## 4.1. AFM with side-view optical imaging

Conventional AFM often integrates with optical microscopes that are configured to have a "bottom-up" view to image cell deformation and labelled cellular proteins, which yields images perpendicular to the loading axis. Such approaches, however, are not able to capture the more substantial cellular deformation and cytoskeletal arrangements that take place along the loading axis. To address this limitation. Chaudhuri et al. developed a side-view AFM to achieve direct. high numerical-aperture epifluorescence side-view imaging of cells (Chaudhuri et al., 2009). This system was first applied to track adhesion between leukocyte and endothelial cells. A leukocyte was attached onto a concanavalin A-coated AFM cantilever and brought into vertical contact with an endothelial cell (Fig. 7a). Aided by side-view fluorescence imaging, the large force rupture events were found to coincide with the return of leukocytes to their steady-state shape, indicating that the detachment of actin cytoskeleton from the membrane was localized to discrete areas, and was responsible for these large force ruptures. Next, this system was used to track adherent cell contraction against an applied load. The contractive force generated by GFP-actin-transfected U20S cells were measured between a fibronectin-coated AFM cantilever and glass substrates, with cell shape and actin cytoskeleton structure monitored simultaneously. This set-up allowed the generation and measurement of contractile forces normal to the surface of adhesion. The resulting inward contraction, as marked by decrease in both cell height and width, evidenced cell contraction as an active behavior.

Subsequently, this system was used to measure the contraction, mechanics, and dynamics of single platelets (Lam et al., 2011). Rapid, high contraction and adhesion forces of individual platelets up to ~ 79 nN were quantified, which was remarkable given their small size compared to myoblasts (~ 300 nN force with three orders of magnitude in volume). The platelet contraction was also found to depend significantly on the stiffness of the microenvironment. It was suggested that the high elasticity and contractile forces of the platelets could contribute to clot stiffening through direct reinforcement by platelets and induce strain-stiffening of fibrins under tension arising from platelet contraction.

This new AFM-fluorescence imaging set-up has shown potential for wide applications in studying cell contractility, cell-cell adhesion, as well as underlying mechanisms such as protein localization, cytoskeletal rearrangement, and possibly nucleus and nucleus-cytoskeleton coupling. A few later studies have further modified and improved the design of side-view IF imaging. For example, as described in Section 3.1, a side-view optical microscope has been

used together with AFM to elucidate the role of Piezo1/2 ion channels in regulating chondrocyte calcium influx under the stimuli of compression and inflammation (Lee et al., 2014; Lee et al., 2021). More recently, prism-based volumetric light sheet fluorescence microscope system was developed to obtain high resolution volumetric imaging during AFM-based mechanical stimuli. It has been applied to capture volumetric images of lysosome trafficking, vimentin nuclear caging, and actin dynamics on the order of one second per single-cell volume, as described in Section 3.2 (Nelsen et al., 2020), and delineation of the roles of chromatin and lamin A/C in nuclear mechanics, as described in Section 3.3 (Hobson et al., 2020), demonstrating its potential in investigating the cell-matrix mechanobiological cross-talk.

## 4.2. AFM with multiple optomicroscopy

Complementing AFM with multiple optical imaging modalities has the potential to acquire simultaneous structural remodeling and functional biomechanical outcomes in live single cells. Trache and Lim integrated an AFM with TIRF and fast-spinning disc (FSD) confocal microscopy for real-time imaging of live cellular mechanotransduction (Trache and Lim, 2009). An openhead AFM scanner with a customized, full-rotation stage was mounted on an inverted microscope platform to preserve all features of a fluorescence microscope. The optical components containing a half wave plate, beam splitter and two illumination ports to enable the white laser to simultaneously feed the illuminators of both TIRF and FSD confocal by singlemode optical fibers (Fig. 7b). This system was applied to study cellular remodeling in vascular smooth muscle cells (VSMCs). VSMCs transfected with mRFP-actin and vinculin-GFP were mechanically stimulated by fibronectin-coated AFM colloidal tips with pN-to-nN-level forces, and TIRF was applied for the real-time tracking of actin filament and vinculin reorganization at the basal cell surface, while FSD confocal was used for monitoring the 3D actin network throughout the entire cell body. As a result, restructuring of actin filaments in the cell body and focal adhesions at cell-substrate contact in response to the mechanical pulling were tracked simultaneously. This microscope was also used to image calcium oscillations in a single liver epithelial cell under AFM stimuli. One suggested potential application was to simultaneously track calcium signaling and its downstream myosin-light-chain (MLC)-dependent cytoskeletal contraction.

This device was then applied to study the role of RhoA-induced cytoskeletal tension in cell remodeling to elucidate the role of tensile stress in vessel wall remodeling (Lim et al., 2012). When tensile stress was induced to VSMCs by fibronectin-coated colloidal tips, cells expressed increased expressions of both actin fibers throughout the cell body and vinculin on the basal cell surface (Fig. 7b). Upon the activation of RhoA, VSMCs exhibited increased stress fiber formation, cell stiffness, integrin activation, myosin phosphorylation, and vice versa. Thus, it was suggested that pre-existing cytoskeletal tension, as mediated by RhoA pathway, governs cell response to external mechanical stimulation. Cells can sense and adapt to the physical microenvironment by a coordinated response of the actomyosin apparatus to establish a new homeostatic state. Their follow-up work further elucidated that the cytoskeletal tension is mediated by RhoA-Src cross-talk, which in turn, induces two distinct force-stiffness functional regimes for integrin  $\alpha_5\beta_1$ -binding to matrix molecules such as fibronectin (Sreenivasappa et al., 2014).

#### 4.3. AFM-FRAP module

Recently, fluorescence recovery after photobleaching, or FRAP, has become an increasingly popular tool in studying the molecular kinetics and dynamics in a spatiotemporal specific manner, where a small region of interest is bleached by a brief exposure to a high-power laser light, and subsequent recovery of fluorescently tagged molecules is monitored over time (Fritzsche and Charras, 2015). Synergistic application of FRAP and AFM could enable the measurement of the turnover dynamics of cellular structures directly underneath the point of contact or any location within the cell volume under real-time application of mechanical stimuli. Skamrahl et al. constructed a new optomechanical AFM-FRAP platform by integrating AFM with a FRAP module (Skamrahl et al., 2019). In this platform, an oil immersion objective on a wide-field fluorescence microscope and FRAP laser unit were connected to the AFM in a bottom-up set-up. Photobleaching was induced in microscopic regions of interest (diameter  $\sim 2 \mu m$ ) via a single laser pulse, enabling the observation of intracellular fluorescence recovery (Fig. 7c).

Under this module, a constant indentation force was applied to the apical actin cortex of live HeLa cells for ~ 150 sec via microspherical tips. In this period, photobleaching was induced, and the turnover of actin and filament lengths of ventral actin stress fibers were then monitored by FRAP (Fig. 7c). The findings showed that the contraction of F-actin fibers in the cortex was mediated by both Arp2/3 and formin, which govern the fluorescence recovery at short and long time scales, respectively. In contrast, actin stress fibers were found to be dominated by formin, consistent with the literature. Increasing applied apical forces from 0.1 to 10 nN was found to significantly increase both the formin-mediated F-actin turnover rate and the stress fiber length, illustrating the adaptative response of actin cytoskeleton to mechanical stimuli. It was suggested this new module could be used to study the mechanoadaptive cytoskeleton remodeling dynamics in other models such as T-cell activation, stem cell differentiation, and cell migration.

#### 4.4. AFM-tensile device

Given the salient mechanosensitivity of cells, probing cell mechanobiology under a controlled external mechanical stress could provide crucial insights into the fundamental processes of mechanotransduction. Both commercial and custom-made cell stretching devices have been developed to work in combination with either optical microscopy or AFM. Hecht et al. designed a uniaxial cell-stretching stage that can be integrated with AFM and fluorescence imaging at the same time (Hecht et al., 2012). A fibronectin-coated polydimethylsiloxane (PDMS) substrate was used for cell culture and adhesion, and the substrate was connected to a motorized stretch device to enable controlled step movement and relaxation. This device was inserted between the AFM head and a bottom-up fluorescence microscope (Fig. 7d). With this device, tensile stretch was applied to squamous cell carcinoma (SCC-25) cells. As a result, strain-dependent change in the cytoskeleton was directly visualized, and the strain-softening effect could be quantified by AFM at the same time (Fig. 7d).

Becerra et al. recently developed a disk-shaped cell stretch device using dielectric elastomer films that can be electro-actuated by the ring-shaped peripheral electrodes (Becerra et al., 2021). With cells seeded in the middle of the elastomer surface, an equi-biaxial or uniaxial tensile strain can be applied to the elastomer using an annular or four-electrode configuration, respectively. Both static and sinusoidal dynamic deformations could be applied to a single adherent cell by controlling the actuating voltage profile. Potential application of this device was demonstrated on T3T fibroblasts and cardiac myocytes. A tensile strain-induced reversible stiffening was found in cardiac myocytes, and high-resolution topography and modulus maps were obtained on fibroblasts to illustrate the long-term stability of the instrument. These proof-of-

concept studies illustrated the potential of tensile devices for studying mechanoadaptation and cytoskeleton remodeling of various cell types.

## 5. Concluding Remarks

Molecular interactions at the cell-matrix interface are crucial biophysical driving forces of cell physiological processes, including proliferation, homeostasis, and disease progression. Understanding this critical microdomain can provide novel targets for disease detection and intervention, as well as tissue regeneration and repair. As outlined by this review, integrated AFM-fluorescence devices have expanded our understanding of this microenvironment by introducing various optics-based changes, transitioning from conventional optical microscopy to more advanced imaging modalities for real-time comprehensive imaging. The coalescence of AFM and fluorescence imaging has progressed to capture many molecular events taking place at the cell-matrix interfaces, including pericellular matrix-mediated mechanotransduction, cytoskeleton remodeling, ion channel activities, and mechanically coupled molecular-level protein expression. This methodology platform thus holds promising potential for addressing many open questions in cell mechanobiology to facilitate disease intervention and regeneration. For example, how do various matrix molecules, e.g., different collagen types and structures, elicit differentiated expressions of specific integrins? How do different integrin types impact cytoskeleton remodeling and nucleus mechanotransduction? How does the proteoglycan and fixed charge microenvironment of the PCM and/or glycocalyx layer regulate the mechanosensing of integrins and ion channels, in addition to the kinetic trap mechanism (Paszek et al., 2014) endowed by glycoproteins? How does inflammation alter cell-matrix interactions that augments focal adhesion, and in turn, progressive fibrosis in scar tissues? Further development and applications of advanced nanomechanical tools, such as multiharmonic AFM (Raman et al., 2011), array-AFM (Yang et al., 2019), 3D-AFM force mapping (Akhtar et al., 2019; Zhou et al., 2020a), as well as parallel cantilever-free probe arrays (Cao et al., 2021), and their wider applications in biological tissues and cells will further expand our understanding of processes at the cell-matrix interface. Collectively, these techniques will benefit the development of novel regeneration or disease modification strategies targeting this critical microdomain.

### Acknowledgment

This work was supported by the National Science Foundation (NSF) Grant CMMI-1751898 to LH, and CMMI-1826202 to MSM and LH, the National Institutes of Health (NIH) Grant AR074490 to LH, as well as Drexel University's Research and Engineering for Pediatrics by Interdisciplinary Collaboration Leveraging Education and Partnerships for Pediatric Healthcare (R-EPIC LEAP for Pediatric Healthcare) from the U.S. Department of Education's Graduate Assistance in Areas of National Need (GAANN) Program (Fellowship Award to NP).

## **Figure Captions**

- Fig. 1. Schematic illustration highlighting several key molecules mediating the interactions at the cell-matrix interface. In the glycocalyx layer, also known as the pericellular domain, both collagen fibrils and fibronectin enable integrin-binding, which in turn regulates the formation of Adhesion Complex (AC) and polymerization of F-actin. Transmembrane constituents such as protein mucin 1 (MUC1), with several phosphorylation sites in its cytoplasmic tail, and receptor CD44, a receptor for hyaluronan (HA), are abundant throughout the cell membrane. Additionally, syndecans, a family of transmembrane proteoglycans, associate with the actin cytoskeleton, growth factors, and integrins through their ectodomain thus activating downstream signaling pathways responsible for a broad range of cellular behavior. Meanwhile, pericellular molecules including large proteoglycans (e.g., aggrecan), small leucine-rich proteoglycans (SLRPs), HA, collagen VI and perlecan, also regulate the integrity of pericellular matrix and the mechanosensitive activities of ion channels. The AC, in conjunction with the mechanosensing of transmembrane moieties and ion channel-mediated cytoskeletal mechanotransduction collectively affect downstream mechanosensitive pathways (e.g., Rho, Rac, MAPK/ERK, YAP/TAZ, β-catenin, etc.), and Linker of Nucleuskeleton and Cytoskeleton (LINC)-mediated nucleus mechanotransduction, which regulates downstream expression of mechanosensitive genes. In the schematic, only a few key matrix and cellular constituents are shown to demonstrate the complexity of cell-matrix mechanobiology and to increase clarity. These illustrated molecules represent general mechanotransduction events at cell-matrix interfaces. and are not specific to individual cell types. The schematic is inspired by Ref. (Afratis et al., 2017; Bourguignon, 2019; Chery et al., 2020; DuFort et al., 2011; Guo et al., 2022; Humphrey et al., 2014; Martino et al., 2018; van Putten and Strijbis, 2017; Wiberg et al., 2002).
- Fig. 2. Micromechanics of the pericellular matrix (PCM) in healthy and osteoarthritis (OA) cartilage via IF-quided AFM nanomechanical mapping. a) Top panel: Schematic illustration of the IF-AFM on cryo-sectioned cartilage. Bottom panel: phase contrast (top) and collagen VI IF (bottom) images highlighting the PCM and territorial/interterritorial extracellular matrix (T/IT-ECM) during AFM tests. Adapted with permission from (Wilusz et al., 2012b). b) Left panel: Representative maps of indentation modulus,  $E_{ind}$ , show reduced PCM modulus in OA cartilage relative to the normal control from human specimens. Middle panel: Comparison of the PCM and T/IT-ECM moduli between normal and OA human cartilage specimens (mean ± 95% CI, 15-16 regions from n = 4 donors, \*: p < 0.05). Right panel: IF images of type VI collagen show increased staining and expansion of collagen VI-labeled PCM domain in OA cartilage. Adapted with permission from (Wilusz et al., 2013). c) Representative maps of  $E_{ind}$  show the early modulus reduction of PCM and T/IT-ECM at 1 week after the destabilization of medial meniscus (DMM) surgery applied to 3-month-old wild-type male mice, relative to the contralateral Sham control. Right panel: Summary of longitudinal changes in the microscale and tissue-level modulus of cartilage from 3 days to 8 weeks after DMM (mean  $\pm$  95% CI,  $n \ge 5$  animals, all the bars are significantly different from the baseline with p < 0.05, unless noted as "n.s.", that is, not significant). Adapted with permission from (Chery et al., 2020).
- **Fig. 3.** Roles of individual matrix molecules in the micromechanics of cartilage pericellular matrix (PCM) via IF-guided AFM nanomechanical mapping. a) Collagen VI. Left panel: Representative IF images of collagen VI show its localization in the PCM of wild-type (WT) cartilage and its absence in *Col6a1*-/- cartilage at 2 months of age. Middle panel: Representative map of indentation modulus obtained on 2-month-old *Col6a1*-/- murine femoral

head cartilage and corresponding perlecan-labeled IF image. Right panel: Comparison of the PCM and T/IT-ECM moduli between WT and  $Col6a1^{-/-}$  cartilage at 2 and 9 months of ages (mean  $\pm$  SEM of  $\geq$  24 sites from n=3 animals, \*: p < 0.05). Adapted with permission from Ref. (Zelenski et al., 2015). b) Decorin. Left panel: Representative IF images of aggrecan and decorin show the reduction of aggrecan and absence of decorin in  $Dcn^{-/-}$  knee cartilage in comparison to WT at 3 months of age. Right panel: Comparison of the PCM and T/IT-ECM moduli between WT and  $Dcn^{-/-}$  cartilage at 3 days, 2 weeks and 3 months of ages (mean  $\pm$  95% CI from n=5 animals, \*: p < 0.001). Adapted with permission from Ref. (Chery et al., 2021). c) Biomimetic proteoglycan (BPG10). Left panel: IF images of adult bovine cartilage explants infiltrated with fluorescently labeled BPG10 and co-stained with collagen VI demonstrate the preferred distribution of BPG10 within the PCM and nearby territorial domain. Right panel: Boxand-whiskers plots of the PCM, T-ECM, and IT-ECM micromodulus for control and BPG10-treated bovine cartilage (> 600 locations for each region, n=5 animals). Each matched pair of circles represents the average modulus of untreated and BPG10-treated cartilage of the same animal. Adapted with permission from Ref. (Kahle et al., 2022).

Fig. 4. Mechanotransduction of chondrocyte Piezo1/2 ion channels measured by AFM and sideview, real-time IF imaging. a) Roles of Piezo1/2 in chondrocyte mechanoresponses to compressive strains. Top panel: Schematic illustration of chondrocyte compression via an AFM tipless cantilever and a representative trace of mechanically activated Ca2+ influx of primary chondrocytes (dotted blue line indicates the time when compression initiates). Sequential sideview IF images show the vertical compression and lateral expansion of an individual chondrocyte under the compression. Bottom panel: Impact of Piezo1/2 knockdown on the maximal Ca<sup>2+</sup> influx of chondrocytes under compression. Left: Chondrocytes treated with Piezo1-targeting or Piezo2-targeting siRNAs (Ps1 and Ps2, mean ± SEM, \*: p < 0.0005 versus respective controls). Right: Chondrocytes treated with piezo-inhibitor GsMXTx4 at 20 µM (Gs20) and 40 µM (Gs40), as well as 2 µM GsMXTx4 with 5 µM dynasore (Gs2+dyn5), the dynamic GTPase inhibitor (mean  $\pm$  SEM, #: p < 0.0005 versus the control). Adapted with permission from Ref. (Lee et al., 2014). b) Roles of Piezo1 in chondrocyte mechanoresponses under inflammatory stimuli. Top panel: Schematic illustration of cyclic chondrocyte compression every 10 seconds via a tipless cantilever and representative traces of mechanically activated Ca<sup>2+</sup> influx of individual chondrocytes with or without the stimulation of 10 ng/mL IL-1a. Bottom panel: Impact of Piezo1 knockdown on the maximal Ca2+ influx of primary chondrocytes under compression and IL-1α stimulation. Left: Chondrocytes treated with Piezo1-targeting siRNA and IL-1α (mean  $\pm$  SEM, \*: p < 0.01). Right: Chondrocytes treated with IL-1α and small molecule inhibitors of specific ion channels, including Piezo1/2 (2 µM GsMTx4 + 5 µM dynasore, GsDy), TRPV4 (25  $\mu$ M GSK205, G205) and VGCC (0.5  $\mu$ M verapamil, Verap) (mean  $\pm$  SEM, #: p < 0.01 versus the IL-1 $\alpha$ -only group, \*: p < 0.0001 between untreated and IL-1 $\alpha$ -only groups). Adapted with permission from Ref. (Lee et al., 2021).

**Fig. 5.** Molecular mechanics of actin networks via customized AFM force spectroscopy and IF imaging. a) Growth of actin networks. Top panel: Schematic illustration of experimental geometry (top) and images of an AFM cantilever before and during polymerization (bottom). In the presence of cytoplasmic extract mix, an ActA-functionalized cantilever activates the Arp2/3 complex and initiates the formation of a branched actin network between the cantilever and glass substrate. Growth of this actin-network deflects the cantilever, which enables the measurement of actin dimensional growth and restoring force exerted by the cantilever. Brightfield image (left) and IF images of rhodamine-labelled actin (middle, right) show the

growth of the actin network at the end of cantilever. Bottom panel: Force-velocity relationship of actin-network growth. Left: A representative length force-time trace curve (red solid line) from a single experiment with the vertical dotted lines marking the transitions between phases A, B and C. The black dotted line in phase b is a linear fit to highlight the load-independence of this phase. Right: Force-velocity relationship for the same experiment shows the load-independent B and stall C phases. Adapted with permission from Ref. (Parekh et al., 2005). b) Reversible stress softening of actin networks. Top panel: AFM-based microrheology of growing dendritic actin networks. Left: Schematic illustration of the experimental set-up, in which, the substrate is driven sinusoidally, and the force transmitted through the network (red mesh) is measured by the AFM cantilever. Middle: IF image of the actin network used for calculating the total actin network area. Right: Corresponding stress and strain curves calculated from the applied sinusoidal loading as a function of time. Bottom panel: Averaged and normalized trace of the nonlinear elasticity of actin networks (mean  $\pm$  STD, n = 28 measurements). Each individual measurement was normalized by the difference between the elasticity before the measurement  $E_{\min}$  and the maximum elasticity for increasing stresses  $E_{\max}$  and  $\sigma_{c}$ . Three distinct regimes of elasticity are identified: linear, stress stiffening, and the reversible stress softening at  $\sigma > \sigma_c$ . Inset: histogram of  $\sigma_c$ , with a mean value of 233 Pa. Adapted with permission from Ref. (Chaudhuri et al., 2007).

Fig. 6. Biomechanics of the nucleus measured by AFM and confocal microscopy. a) Puncture of plasma and nuclear membrane by AFM needle tip on HeLa cells expressing CHMP4B-GFP. Left panel: Top: Schematic illustration of probing isolated CHMP4B-eGFP HeLa cells with the needle tip. Bottom: Representative force-distance curve indicating force-relaxation regions corresponding to combined membrane puncture (A), retraction of probe from nuclear membrane (B), and retraction of probe from plasma membrane (C) (Inset: SEM image of an AFM needle tip). A fluorescent z-stack reconstruction image (1) before needle puncture reveals the small (≈ 1 µm) distance between plasma and nuclear membranes, matching observations of the forcerelaxation curve. (2) Indirect visualization of the AFM needle-tip (pink) and CHMP4B recruitment at the puncture site (green) within the nucleus (blue) during needle puncture. Right panel: Top: Representative fluorescence images of CHMP4B at 1, 5 and 10 minutes after puncture. Bottom: Relative fluorescence intensity of HeLa CHMP4B-eGFP cells (n = 10, mean  $\pm$  SEM) probed with a needle tip versus a microspherical tip. Adapted with permission from Ref. (McCreery et al., 2021). b) 3D nanomechanical mapping of the nucleolus biomechanics of NIH 3T3 fibroblast and MDA-MB-231 breast cancer cells. Left panel: Top: SEM image of a representative long carbon tip (left inset: a parabolic fit for tip radius estimation; right inset: a regular pyramidal tip of the same cantilever type for comparison). Bottom: Vertical cross-section of confocal z-stack images along the marked lines in the right panel show the size and depth of the nucleoli (red) and cell shape (F-actin, green). Right panel: Representative nanomechanical maps of E<sub>storage</sub> and confocal images of nucleoli (SYTO85 staining) show the higher storage modulus at the nucleoli of both cell types. Adapted with permission from Ref. (Efremov et al., 2022).

**Fig. 7.** Custom-built devices that integrate AFM nanomechanical testing and IF imaging. a) AFM with side-view optical imaging. Top panel: Left: Schematic illustration of side-view imaging path and desired image of sample (dotted line: image plane). Right: A bright-field and merged IF side-view images of a U2OS cell showing cell membrane (red), GFP-actin (green) and the stained nucleus (blue). Dotted lines: substrate surface. Bottom panel: Schematic illustration of the measurement of adhesion between a leukocyte (red) and an endothelial cell (green), and representative images of the leukocyte labeled with a membrane dye taken at the indicated

distances. White arrows: tethers between the two cells. Right: Force (red) and corresponding aspect ratio of the cell (black, dimensions illustrated in the inset) measured for all the images taken with the side-view imaging path. Adapted with permission from Ref. (Chaudhuri et al., 2009). b) AFM with multiple optomicroscopy. Top panel: Picture shows the integrated design with AFM scanner, TIRF and confocal microscopes, and schematic illustration of tensile stretching of a vascular smooth muscle cell (VSMC) in vitro via a fibronectin-coated microspherical AFM tip. Bottom panel: Representative TIRF and confocal images of VSMC coexpressing vinculin-GFP (green) and actin-mRFP (red) before and after stimulation by a fibronectin-coated AFM tip. White arrow heads: actin fibers undergoing appreciable disassembly (big arrow heads) or assembly (small arrow heads) in response to the stimulation. Adapted with permission from Ref. (Lim et al., 2012; Trache and Lim, 2009). c) AFM with the FRAP module. Top panel: Schematic illustration of the AFM-FRAP setup for simultaneous quantification of molecule kinetics and cell mechanics. Bottom panel: Application of AFM-FRAP in ventral actin stress fibers. Representative map of indentation slope on a HeLa cell, and time-series of FRAP kymographs of ventral actin stress fibers of a HeLa cell in response to 10 nN external applied force. Adapted with permission from Ref. (Skamrahl et al., 2019). d) AFM with the tensile stretching device. Top panel: Image of the cell stretching device (see original reference for the legends of different device parts a-g), and schematic illustration of the integrated assembly including the stretching device, top-down AFM head, and inverted microscope. Bottom panel: Structure and mechanics of squamous cell carcinoma (SCC)-25 cells under tension. Left: Cytokeratin IF images of living SCC-25 cells showing cell tensile deformation. Right: Corresponding modulus maps showing the reduction of modulus at 20% cell stretching of SCC-25 cells. White arrows: keratin domains with higher modulus before deformation. Adapted with permission from Ref. (Hecht et al., 2012).

#### References

- A-Hassan, E., Heinz, W.F., Antonik, M.D., D'Costa, N.P., Nageswaran, S., Schoenenberger, C.A., Hoh, J.H., 1998. Relative microelastic mapping of living cells by atomic force microscopy. Biophys. J. 74, 1564-1578.
- Abu-Lail, N.I., Ohashi, T., Clark, R.L., Erickson, H.P., Zauscher, S., 2006. Understanding the elasticity of fibronectin fibrils: unfolding strengths of FN-III and GFP domains measured by single molecule force spectroscopy. Matrix Biol. 25, 175-184.
- Afratis, N.A., Nikitovic, D., Multhaupt, H.A., Theocharis, A.D., Couchman, J.R., Karamanos, N.K., 2017. Syndecans key regulators of cell signaling and biological functions. FEBS J 284, 27-41.
- Akhtar, I., Rehman, M.A., Choi, W., Kumar, S., Lee, N., Cho, S.-J., Park, H.-H., Park, K.-H., Seo, Y.J.A.S.S., 2019. Three-dimensional atomic force microscopy for ultra-high-aspect-ratio imaging. Appl. Surf. Sci. 469, 582-592.
- Alexopoulos, L.G., Youn, I., Bonaldo, P., Guilak, F., 2009. Developmental and osteoarthritic changes in Col6a1-knockout mice: biomechanics of type VI collagen in the cartilage pericellular matrix. Arthritis Rheumatol. 60, 771-779.
- Ando, T., Uchihashi, T., Kodera, N., 2013. High-speed AFM and applications to biomolecular systems. Annu. Rev. Biophys. 42, 393-414.
- Azadi, M., Nia, H.T., Gauci, S.J., Ortiz, C., Fosang, A.J., Grodzinsky, A.J., 2016. Wide bandwidth nanomechanical assessment of murine cartilage reveals protection of aggrecan knock-in mice from joint-overuse. J. Biomech. 49, 1634-1640.
- Barbee, K.A., Mundel, T., Lal, R., Davies, P.F., 1995. Subcellular distribution of shear stress at the surface of flow-aligned and nonaligned endothelial monolayers. Am. J. Physiol. 268, H1765-1772.
- Batista, M.A., Nia, H.T., Önnerfjord, P., Cox, K.A., Ortiz, C., Grodzinsky, A.J., Heinegård, D., Han, L., 2014. Nanomechanical phenotype of chondroadherin-null murine articular cartilage. Matrix Biol. 38, 84-90.
- Becerra, N., Salis, B., Tedesco, M., Moreno Flores, S., Vena, P., Raiteri, R., 2021. AFM and fluorescence microscopy of single cells with simultaneous mechanical stimulation via electrically stretchable substrates. Materials (Basel) 14, 4131.
- Beicker, K., O'Brien, E.T., 3rd, Falvo, M.R., Superfine, R., 2018. Vertical light sheet enhanced side-view imaging for AFM cell mechanics studies. Sci. Rep. 8, 1504.
- Binnig, G., Quate, C.F., Gerber, C., 1986. Atomic force microscope. Phys. Rev. Lett. 56, 930-933.
- Birk, D.E., Brückner, P., 2011. Collagens, suprastructures, and collagen fibril assembly, in: Mecham, R.P. (Ed.), The Extracellular Matrix: an Overview. Springer-Verlag, Berlin, pp. 77-115
- Bourguignon, L.Y.W., 2019. Matrix hyaluronan-cd44 interaction activates microrna and Incrna signaling associated with chemoresistance, invasion, and tumor progression. Front. Oncol. 9, 492.
- Cao, W., Alsharif, N., Huang, Z., White, A.E., Wang, Y., Brown, K.A., 2021. Massively parallel cantilever-free atomic force microscopy. Nat. Commun. 12, 393.
- Cascione, M., de Matteis, V., Rinaldi, R., Leporatti, S., 2017. Atomic force microscopy combined with optical microscopy for cells investigation. Microsc. Res. Tech. 80, 109-123.
- Cazaux, S., Sadoun, A., Biarnes-Pelicot, M., Martinez, M., Obeid, S., Bongrand, P., Limozin, L., Puech, P.H., 2016. Synchronizing atomic force microscopy force mode and fluorescence microscopy in real time for immune cell stimulation and activation studies. Ultramicroscopy 160, 168-181.
- Chandrasekaran, P., Kwok, B., Han, B., Adams, S.M., Wang, C., Chery, D.R., Mauck, R.L., Dyment, N.A., Lu, X.L., Frank, D.B., Koyama, E., Birk, D.E., Han, L., 2021. Type V collagen

- regulates the structure and biomechanics of TMJ condylar cartilage: a fibrous-hyaline hybrid. Matrix Biol. 102, 1-19.
- Charras, G.T., Horton, M.A., 2002. Single cell mechanotransduction and its modulation analyzed by atomic force microscope indentation. Biophys. J. 82, 2970-2981.
- Charras, G.T., Lehenkari, P.P., Horton, M.A., 2001. Atomic force microscopy can be used to mechanically stimulate osteoblasts and evaluate cellular strain distributions. Ultramicroscopy 86, 85-95.
- Chaudhuri, O., Parekh, S.H., Fletcher, D.A., 2007. Reversible stress softening of actin networks. Nature 445, 295-298.
- Chaudhuri, O., Parekh, S.H., Lam, W.A., Fletcher, D.A., 2009. Combined atomic force microscopy and side-view optical imaging for mechanical studies of cells. Nat. Methods 6, 383-387.
- Chery, D.R., Han, B., Li, Q., Zhou, Y., Heo, S.J., Kwok, B., Chandrasekaran, P., Wang, C., Qin, L., Lu, X.L., Kong, D., Enomoto-Iwamoto, M., Mauck, R.L., Han, L., 2020. Early changes in cartilage pericellular matrix micromechanobiology portend the onset of post-traumatic osteoarthritis. Acta Biomater. 111, 267- 278.
- Chery, D.R., Han, B., Zhou, Y., Wang, C., Adams, S.M., Chandrasekaran, P., Kwok, B., Heo, S.J., Enomoto-Iwamoto, M., Lu, X.L., Kong, D., Iozzo, R.V., Birk, D.E., Mauck, R.L., Han, L., 2021. Decorin regulates cartilage pericellular matrix micromechanobiology. Matrix Biol. 96, 1-17.
- Christensen, S.E., Coles, J.M., Zelenski, N.A., Furman, B.D., Leddy, H.A., Zauscher, S., Bonaldo, P., Guilak, F., 2012. Altered trabecular bone structure and delayed cartilage degeneration in the knees of collagen VI null mice. PLoS One 7, e33397.
- Clapham, D.E., 2007. Calcium signaling. Cell 131, 1047-1058.
- Coles, J.M., Blum, J.J., Jay, G.D., Darling, E.M., Guilak, F., Zauscher, S., 2008. In situ friction measurement on murine cartilage by atomic force microscopy. J. Biomech. 41, 541-548.
- Connizzo, B.K., Grodzinsky, A.J., 2018. Multiscale poroviscoelastic compressive properties of mouse supraspinatus tendons are altered in young and aged mice. J. Biomech. Eng. 140, 0510021-0510028.
- Danalache, M., Kleinert, R., Schneider, J., Erler, A.L., Schwitalle, M., Riester, R., Traub, F., Hofmann, U.K., 2019. Changes in stiffness and biochemical composition of the pericellular matrix as a function of spatial chondrocyte organisation in osteoarthritic cartilage. Osteoarthr. Cartil. 27, 823-832.
- Darling, E.M., Wilusz, R.E., Bolognesi, M.P., Zauscher, S., Guilak, F., 2010. Spatial mapping of the biomechanical properties of the pericellular matrix of articular cartilage measured in situ via atomic force microscopy. Biophys. J. 98, 2848-2856.
- Dean, D., Han, L., Grodzinsky, A.J., Ortiz, C., 2006. Compressive nanomechanics of opposing aggrecan macromolecules. J. Biomech. 39, 2555-2565.
- Doyran, B., Tong, W., Li, Q., Jia, H., Zhang, X., Chen, C., Enomoto-Iwamoto, M., Lu, X.L., Qin, L., Han, L., 2017. Nanoindentation modulus of murine cartilage: a sensitive indicator of the initiation and progression of post-traumatic osteoarthritis. Osteoarthr. Cartil. 25, 108-117.
- DuFort, C.C., Paszek, M.J., Weaver, V.M., 2011. Balancing forces: architectural control of mechanotransduction. Nat. Rev. Mol. Cell Biol. 12, 308-319.
- Efremov, Y.M., Suter, D.M., Timashev, P.S., Raman, A., 2022. 3D nanomechanical mapping of subcellular and sub-nuclear structures of living cells by multi-harmonic AFM with long-tip microcantilevers. Sci. Rep. 12, 529.
- Efremov, Y.M., Velay-Lizancos, M., Weaver, C.J., Athamneh, A.I., Zavattieri, P.D., Suter, D.M., Raman, A., 2019. Anisotropy vs isotropy in living cell indentation with AFM. Sci. Rep. 9, 5757.
- Ferreira, S.A., Motwani, M.S., Faull, P.A., Seymour, A.J., Yu, T.T.L., Enayati, M., Taheem, D.K., Salzlechner, C., Haghighi, T., Kania, E.M., Oommen, O.P., Ahmed, T., Loaiza, S., Parzych,

- K., Dazzi, F., Varghese, O.P., Festy, F., Grigoriadis, A.E., Auner, H.W., Snijders, A.P., Bozec, L., Gentleman, E., 2018. Bi-directional cell-pericellular matrix interactions direct stem cell fate. Nat. Commun. 9 4049.
- Formigli, L., Meacci, E., Sassoli, C., Chellini, F., Giannini, R., Quercioli, F., Tiribilli, B., Squecco, R., Bruni, P., Francini, F., Zecchi-Orlandini, S., 2005. Sphingosine 1-phosphate induces cytoskeletal reorganization in C2C12 myoblasts: physiological relevance for stress fibres in the modulation of ion current through stretch-activated channels. J. Cell. Sci. 118, 1161-1171.
- Fritzsche, M., Charras, G., 2015. Dissecting protein reaction dynamics in living cells by fluorescence recovery after photobleaching. Nat. Protoc. 10, 660-680.
- Gavara, N., Chadwick, R.S., 2016. Relationship between cell stiffness and stress fiber amount, assessed by simultaneous atomic force microscopy and live-cell fluorescence imaging. Biomech. Model. Mechanobiol. 15, 511-523.
- Glasson, S.S., Blanchet, T.J., Morris, E.A., 2007. The surgical destabilization of the medial meniscus (DMM) model of osteoarthritis in the 129/SvEv mouse. Osteoarthr. Cartil. 15, 1061-1069.
- Guilak, F., Hayes, A.J., Melrose, J., 2021. Perlecan in pericellular mechanosensory cell-matrix communication, extracellular matrix stabilisation and mechanoregulation of load-bearing connective tissues. Int. J. Mol. Sci. 22, 2716.
- Guilak, F., Nims, R.J., Dicks, A., Wu, C.L., Meulenbelt, I., 2018. Osteoarthritis as a disease of the cartilage pericellular matrix. Matrix Biol. 71-72, 40-50.
- Guo, Q., Yang, C., Gao, F., 2022. The state of CD44 activation in cancer progression and therapeutic targeting. FEBS J. In press, doi: 10.1111/febs.16179.
- Haase, K., Macadangdang, J.K., Edrington, C.H., Cuerrier, C.M., Hadjiantoniou, S., Harden, J.L., Skerjanc, I.S., Pelling, A.E., 2016. Extracellular forces cause the nucleus to deform in a highly controlled anisotropic manner. Sci. Rep. 6, 21300.
- Han, B., Li, Q., Wang, C., Chandrasekaran, P., Zhou, Y., Qin, L., Liu, X.S., Enomoto-Iwamoto, M., Kong, D., Iozzo, R.V., Birk, D.E., Han, L., 2021. Differentiated activities of decorin and biglycan in the progression of post-traumatic osteoarthritis. Osteoarthr. Cartil. 29, 1181-1192.
- Han, B., Li, Q., Wang, C., Patel, P., Adams, S.M., Doyran, B., Nia, H.T., Oftadeh, R., Zhou, S., Li, C.Y., Liu, X.S., Lu, X.L., Enomoto-Iwamoto, M., Qin, L., Mauck, R.L., Iozzo, R.V., Birk, D.E., Han, L., 2019. Decorin regulates the aggrecan network integrity and biomechanical functions of cartilage extracellular matrix. ACS Nano 13, 11320-11333.
- Han, B., Nia, H.T., Wang, C., Chandrasekaran, P., Li, Q., Chery, D.R., Li, H., Grodzinsky, A.J., Han, L., 2017. AFM-nanomechanical test: an interdisciplinary tool that links the understanding of cartilage and meniscus biomechanics, osteoarthritis degeneration and tissue engineering. ACS Biomater. Sci. Eng. 3, 2033-2049.
- Han, L., Dean, D., Daher, L.A., Grodzinsky, A.J., Ortiz, C., 2008. Cartilage aggrecan can undergo self-adhesion. Biophys. J. 95, 4862-4870.
- Han, L., Dean, D., Mao, P., Ortiz, C., Grodzinsky, A.J., 2007a. Nanoscale shear deformation mechanisms of opposing cartilage aggrecan macromolecules. Biophys. J. 93, L23-L25.
- Han, L., Dean, D., Ortiz, C., Grodzinsky, A.J., 2007b. Lateral nanomechanics of cartilage aggrecan macromolecules. Biophys. J. 92, 1384-1398.
- Han, L., Frank, E.H., Greene, J.J., Lee, H.-Y., Hung, H.-H.K., Grodzinsky, A.J., Ortiz, C., 2011a. Time-dependent nanomechanics of cartilage. Biophys. J. 100, 1846-1854.
- Han, L., Grodzinsky, A.J., Ortiz, C., 2011b. Nanomechanics of the cartilage extracellular matrix. Annu. Rev. Mater. Res. 41, 133-168.
- Hecht, E., Knittel, P., Felder, E., Dietl, P., Mizaikoff, B., Kranz, C., 2012. Combining atomic force-fluorescence microscopy with a stretching device for analyzing mechanotransduction processes in living cells. Analyst 137, 5208-5214.

- Heinegård, D., 2009. Proteoglycans and more from molecules to biology. Int. J. Exp. Pathol. 90, 575-586.
- Heinegård, D., Saxne, T., 2011. The role of the cartilage matrix in osteoarthritis. Nat. Rev. Rheumatol. 7, 50-56.
- Heo, S.J., Cosgrove, B.D., Dai, E.N., Mauck, R.L., 2018. Mechano-adaptation of the stem cell nucleus. Nucleus 9, 9-19.
- Hobson, C.M., Kern, M., O'Brien, E.T., 3rd, Stephens, A.D., Falvo, M.R., Superfine, R., 2020. Correlating nuclear morphology and external force with combined atomic force microscopy and light sheet imaging separates roles of chromatin and lamin A/C in nuclear mechanics. Mol. Biol. Cell 31, 1788-1801.
- Hosseininia, S., Weis, M.A., Rai, J., Kim, L., Funk, S., Dahlberg, L.E., Eyre, D.R., 2016. Evidence for enhanced collagen type III deposition focally in the territorial matrix of osteoarthritic hip articular cartilage. Osteoarthr. Cartil. 24, 1029-1035.
- Humphrey, J.D., Dufresne, E.R., Schwartz, M.A., 2014. Mechanotransduction and extracellular matrix homeostasis. Nat. Rev. Mol. Cell Biol. 15, 802-812.
- Jacobs, T.D.B., Gotsmann, B., Lantz, M.A., Carpick, R.W., 2010. On the application of transition state theory to atomic-scale wear. Tribol. Lett. 39, 257-271
- Jin, P., Jan, L.Y., Jan, Y.N., 2020. Mechanosensitive ion channels: structural features relevant to mechanotransduction mechanisms. Annu. Rev. Neurosci. 43, 207-229.
- Johnson, K.L., 1985. Contact Mechanics. Cambridge University Press, Cambridge, UK.
- Jonas, O., Duschl, C., 2010. Force propagation and force generation in cells. Cytoskeleton 67, 555-563.
- Jung, S.H., Park, D., Park, J.H., Kim, Y.M., Ha, K.S., 2010. Molecular imaging of membrane proteins and microfilaments using atomic force microscopy. Exp. Mol. Med. 42, 597-605.
- Kahle, E.R., Han, B., Chandrasekaran, P., Phillips, E.R., Mulcahey, M.K., Lu, X.L., Marcolongo, M.S., Han, L., 2022. Molecular engineering of pericellular microniche via biomimetic proteoglycans modulates cell mechanobiology. ACS Nano 16, 1220-1230.
- Kawamoto, T., Kawamoto, K., 2014. Preparation of thin frozen sections from nonfixed and undecalcified hard tissues using Kawamot's film method (2012). Methods Mol. Biol. 1130, 149-164.
- Kiio, T.M., Park, S., 2020. Nano-scientific application of atomic force microscopy in pathology: From molecules to tissues. Int. J. Med. Sci. 17 844-858.
- Krause, M., Te Riet, J., Wolf, K., 2013. Probing the compressibility of tumor cell nuclei by combined atomic force-confocal microscopy. Phys. Biol. 10, 065002.
- Krieg, M., Fläschner, G., Alsteens, D., Gaub, B.M., Roos, W.H., Wuite, G.J.L., Gaub, H.E., Gerber, C., Dufrêne, Y.F., Müller, D.J., 2019. Atomic force microscopy-based mechanobiology. Nat. Rev. Phys. 1, 41-57.
- Kronlage, C., Schäfer-Herte, M., Böning, D., Oberleithner, H., Fels, J., 2015. Feeling for filaments: quantification of the cortical actin web in live vascular endothelium. Biophys. J. 109, 687-698.
- Kuo, J.C., Paszek, M.J., 2021. Glycocalyx curving the membrane: forces emerging from the cell exterior. Annu. Rev. Cell Dev. Biol. 37, 257-283.
- Lam, W.A., Chaudhuri, O., Crow, A., Webster, K.D., Li, T.D., Kita, A., Huang, J., Fletcher, D.A., 2011. Mechanics and contraction dynamics of single platelets and implications for clot stiffening. Nat. Mater. 10, 61-66.
- Lee, W., Leddy, H.A., Chen, Y., Lee, S.H., Zelenski, N.A., McNulty, A.L., Wu, J., Beicker, K.N., Coles, J., Zauscher, S., Grandl, J., Sachs, F., Guilak, F., 2014. Synergy between Piezo1 and Piezo2 channels confers high-strain mechanosensitivity to articular cartilage. Proc. Natl. Acad. Sci. U. S. A. 111, E5114-5122.
- Lee, W., Nims, R.J., Savadipour, A., Zhang, Q., Leddy, H.A., Liu, F., McNulty, A.L., Chen, Y., Guilak, F., Liedtke, W.B., 2021. Inflammatory signaling sensitizes Piezo1

- mechanotransduction in articular chondrocytes as a pathogenic feed-forward mechanism in osteoarthritis. Proc. Natl. Acad. Sci. U. S. A. 118, e2001611118.
- Li, M., Dang, D., Liu, L., Xi, N., Wang, Y., 2017. Atomic force microscopy in characterizing cell mechanics for biomedical applications: a review. IEEE Trans. Nanobioscience 16, 523-540.
- Li, Q., Han, B., Wang, C., Tong, W., Tseng, W.J., Han, L.-H., Liu, X.S., Enomoto-Iwamoto, M., Mauck, R.L., Qin, L., Iozzo, R.V., Birk, D.E., Han, L., 2020. Mediation of cartilage matrix degeneration and fibrillation by decorin in post-traumatic osteoarthritis. Arthritis Rheumatol. 72. 1266-1277.
- Li, Z., Lee, H., Zhu, C., 2016. Molecular mechanisms of mechanotransduction in integrin-mediated cell-matrix adhesion. Exp. Cell Res. 349, 85-94.
- Liang, W., Shi, H., Yang, X., Wang, J., Yang, W., Zhang, H., Liu, L., 2020. Recent advances in AFM-based biological characterization and applications at multiple levels. Soft Matter 16, 8962-8984.
- Lim, S.M., Trzeciakowski, J.P., Sreenivasappa, H., Dangott, L.J., Trache, A., 2012. RhoA-induced cytoskeletal tension controls adaptive cellular remodeling to mechanical signaling. Integr. Biol. 4, 615-627.
- Lin, D.C., Horkay, F., 2008. Nanomechanics of polymer gels and biological tissues: a critical review of analytical approaches in the Hertzian regime and beyond. Soft Matter 4, 669-682.
- Liu, H., Wen, J., Xiao, Y., Liu, J., Hopyan, S., Radisic, M., Simmons, C.A., Sun, Y., 2014. In situ mechanical characterization of the cell nucleus by atomic force microscopy. ACS Nano 8, 3821-3828.
- Loebel, C., Kwon, M.Y., Wang, C., Han, L., Mauck, R.L., Burdick, J.A., 2020. Metabolic labeling to probe the spatiotemporal accumulation of matrix at the chondrocyte-hydrogel interface. Adv. Funct. Mater. 30, 1909802.
- Loebel, C., Mauck, R.L., Burdick, J.A., 2019. Local nascent protein deposition and remodelling guide mesenchymal stromal cell mechanosensing and fate in three-dimensional hydrogels. Nat. Mater. 18, 883-891.
- Martinac, B., 2004. Mechanosensitive ion channels: molecules of mechanotransduction. J. Cell. Sci. 117, 2449-2460.
- Martino, F., Perestrelo, A.R., Vinarský, V., Pagliari, S., Forte, G., 2018. Cellular mechanotransduction: from tension to function. Front. Physiol. 9, 824.
- Mattice, J.M., Lau, A.G., Oyen, M.L., Kent, R.W., 2006. Spherical indentation load-relaxation of soft biological tissues. J. Mater. Res. 21, 2003-2010.
- McCreery, K.P., Xu, X., Scott, A.K., Fajrial, A.K., Calve, S., Ding, X., Neu, C.P., 2021. Nuclear stiffness decreases with disruption of the extracellular matrix in living tissues. Small 17, e2006699.
- McLeod, C.M., Mauck, R.L., 2016. High fidelity visualization of cell-to-cell variation and temporal dynamics in nascent extracellular matrix formation. Sci. Rep. 6, 38852.
- McLeod, M.A., Wilusz, R.E., Guilak, F., 2013. Depth-dependent anisotropy of the micromechanical properties of the extracellular and pericellular matrices of articular cartilage evaluated via atomic force microscopy. J. Biomech. 46, 586-592.
- Möckl, L., 2020. The emerging role of the mammalian glycocalyx in functional membrane organization and immune system regulation. Front. Cell Dev. Biol. 8, 253.
- Nelsen, E., Hobson, C.M., Kern, M.E., Hsiao, J.P., O'Brien Iii, E.T., Watanabe, T., Condon, B.M., Boyce, M., Grinstein, S., Hahn, K.M., Falvo, M.R., Superfine, R., 2020. Combined atomic force microscope and volumetric light sheet system for correlative force and fluorescence mechanobiology studies. Sci. Rep. 10, 8133.
- Nia, H.T., Bozchalooi, I.S., Li, Y., Han, L., Hung, H.-H., Frank, E.H., Youcef-Toumi, K., Ortiz, C., Grodzinsky, A.J., 2013. High-bandwidth AFM-based rheology reveals that cartilage is most sensitive to high loading rates at early stages of impairment. Biophys. J. 104, 1529-1537.

- Oberhauser, A.F., Marszalek, P.E., Erickson, H.P., Fernandez, J.M., 1998. The molecular elasticity of the extracellular matrix protein tenascin. Nature 393, 181-185.
- Ozkan, A.D., Topal, A.E., Dana, A., Guler, M.O., Tekinay, A.B., 2016. Atomic force microscopy for the investigation of molecular and cellular behavior. Micron 89, 60-76.
- Parekh, S.H., Chaudhuri, O., Theriot, J.A., Fletcher, D.A., 2005. Loading history determines the velocity of actin-network growth. Nat. Cell Biol. 7, 1219-1223.
- Paszek, M.J., DuFort, C.C., Rossier, O., Bainer, R., Mouw, J.K., Godula, K., Hudak, J.E., Lakins, J.N., Wijekoon, A.C., Cassereau, L., Rubashkin, M.G., Magbanua, M.J., Thorn, K.S., Davidson, M.W., Rugo, H.S., Park, J.W., Hammer, D.A., Giannone, G., Bertozzi, C.R., Weaver, V.M., 2014. The cancer glycocalyx mechanically primes integrin-mediated growth and survival. Nature 511, 319-325.
- Prudnikova, K., Lightfoot Vidal, S.E., Sarkar, S., Yu, T., Yucha, R.W., Ganesh, N., Penn, L.S., Han, L., Schauer, C.L., Vresilovic, E.J., Marcolongo, M.S., 2018. Aggrecan-like biomimetic proteoglycans (BPGs) composed of natural chondroitin sulfate bristles grafted onto a poly(acrylic acid) core for molecular engineering of the extracellular matrix. Acta Biomater. 75, 93-104.
- Prudnikova, K., Yucha, R.W., Patel, P., Kriete, A.S., Han, L., Penn, L.S., Marcolongo, M.S., 2017. Biomimetic proteoglycans mimic macromolecular architecture and water uptake of natural proteoglycans. Biomacromolecules 18, 1713-1723.
- Quinn, T.M., Maung, A.A., Grodzinsky, A.J., Hunziker, E.B., Sandy, J.D., 1999. Physical and biological regulation of proteoglycan turnover around chondrocytes in cartilage explants. Implications for tissue degradation and repair. Ann. N. Y. Acad. Sci. 878, 420-441.
- Raman, A., Trigueros, S., Cartagena, A., Stevenson, A.P., Susilo, M., Nauman, E., Contera, S.A., 2011. Mapping nanomechanical properties of live cells using multi-harmonic atomic force microscopy. Nat. Nanotechnol. 6, 809-814.
- Rief, M., Gautel, M., Oesterhelt, F., Fernandez, J.M., Gaub, H.E., 1997. Reversible unfolding of individual titin immunoglobulin domains by AFM. Science 276, 1109-1112.
- Rojas, F.P., Batista, M.A., Lindburg, C.A., Dean, D., Grodzinsky, A.J., Ortiz, C., Han, L., 2014. Molecular adhesion between cartilage extracellular matrix macromolecules. Biomacromolecules 15, 772-780.
- Rosenbluth, M.J., Crow, A., Shaevitz, J.W., Fletcher, D.A., 2008. Slow stress propagation in adherent cells. Biophys. J. 95, 6052-6059.
- Rux, C.J., Vahidi, G., Darabi, A., Cox, L.M., Heveran, C.M., 2022. Perilacunar bone tissue exhibits sub-micrometer modulus gradation which depends on the recency of osteocyte bone formation in both young adult and early-old-age female C57Bl/6 mice. Bone 157, 116327.
- Sanchez-Adams, J., Wilusz, R.E., Guilak, F., 2013. Atomic force microscopy reveals regional variations in the micromechanical properties of the pericellular and extracellular matrices of the meniscus. J. Orthop. Res. 31, 1218-1225.
- Seetharaman, S., Etienne-Manneville, S., 2018. Integrin diversity brings specificity in mechanotransduction. Biol. Cell 110, 49-64.
- Sen, S., Kumar, S., 2010. Combining mechanical and optical approaches to dissect cellular mechanobiology. J. Biomech. 43, 45-54.
- Silberberg, Y.R., Pelling, A.E., Yakubov, G.E., Crum, W.R., Hawkes, D.J., Horton, M.A., 2008. Mitochondrial displacements in response to nanomechanical forces. J. Mol. Recognit. 21, 30-36.
- Singer, I., Kawka, D.W., Bayne, E.K., Donatelli, S.A., Weidner, J.R., Williams, H.R., Ayala, J.M., Mumford, R.A., Lark, M.W., Glant, T.T., 1995. VDIPEN, a metalloproteinase-generated neoepitope, is induced and immunolocalized in articular cartilage during inflammatory arthritis. J. Clin. Investig. 95, 2178-2186.

- Skamrahl, M., Colin-York, H., Barbieri, L., Fritzsche, M., 2019. Simultaneous quantification of the interplay between molecular turnover and cell mechanics by AFM-FRAP. Small 15, e1902202.
- Sreenivasappa, H., Chaki, S.P., Lim, S.M., Trzeciakowski, J.P., Davidson, M.W., Rivera, G.M., Trache, A., 2014. Selective regulation of cytoskeletal tension and cell-matrix adhesion by RhoA and Src. Integr. Biol. 6, 743-754.
- Staunton, J.R., Doss, B.L., Lindsay, S., Ros, R., 2016. Correlating confocal microscopy and atomic force indentation reveals metastatic cancer cells stiffen during invasion into collagen I matrices. Sci. Rep. 6, 19686.
- Sun, Z., Guo, S.S., Fässler, R., 2016. Integrin-mediated mechanotransduction. J. Cell. Biol. 215, 445-456.
- Tai, K., Dao, M., Suresh, S., Palazoglu, A., Ortiz, C., 2007. Nanoscale heterogeneity promotes energy dissipation in bone. Nat. Mater. 6, 454-462.
- Trache, A., Lim, S.M., 2009. Integrated microscopy for real-time imaging of mechanotransduction studies in live cells. J. Biomed. Opt. 14, 034024.
- van Putten, J.P.M., Strijbis, K., 2017. Transmembrane mucins: Signaling receptors at the intersection of inflammation and cancer. J. Innate Immun. 9, 281-299.
- Vincent, T.L., McLean, C.J., Full, L.E., Peston, D., Saklatvala, J., 2007. FGF-2 is bound to perlecan in the pericellular matrix of articular cartilage, where it acts as a chondrocyte mechanotransducer. Osteoarthr. Cartil. 15, 752-763.
- Wang, C., Brisson, B.K., Terajima, M., Li, Q., Hoxha, K., Han, B., Goldberg, A.M., Liu, X.S., Marcolongo, M.S., Enomoto-Iwamoto, M., Yamauchi, M., Volk, S.W., Han, L., 2020. Type III collagen is a key regulator of the collagen fibrillar structure and biomechanics of articular cartilage and meniscus. Matrix Biol. 85-86, 47-67.
- Wang, T., Lai, J.H., Yang, F., 2016. Effects of hydrogel stiffness and extracellular compositions on modulating cartilage regeneration by mixed populations of stem cells and chondrocytes in vivo. Tissue Eng. Part A 22, 1348-1356.
- Watanabe-Nakayama, T., Machida, S.I., Harada, I., Sekiguchi, H., Afrin, R., Ikai, A., 2011. Direct detection of cellular adaptation to local cyclic stretching at the single cell level by atomic force microscopy. Biophys. J. 100, 564-572.
- Wiberg, C., Heinegard, D., Wenglen, C., Timpl, R., Morgelin, M., 2002. Biglycan organizes collagen VI into hexagonal-like networks resembling tissue structures. J. Biol. Chem. 277, 49120-49126.
- Wilusz, R.E., Defrate, L.E., Guilak, F., 2012a. A biomechanical role for perlecan in the pericellular matrix of articular cartilage. Matrix Biol. 31, 320-327.
- Wilusz, R.E., DeFrate, L.E., Guilak, F., 2012b. Immunofluorescence-guided atomic force microscopy to measure the micromechanical properties of the pericellular matrix of porcine articular cartilage. J. R. Soc. Interface 9, 2997-3007.
- Wilusz, R.E., Guilak, F., 2014. High resistance of the mechanical properties of the chondrocyte pericellular matrix to proteoglycan digestion by chondroitinase, aggrecanase, or hyaluronidase. J. Mech. Behav. Biomed. Mater. 38, 183-197.
- Wilusz, R.E., Sanchez-Adams, J., Guilak, F., 2014. The structure and function of the pericellular matrix of articular cartilage. Matrix Biol. 39 25-32.
- Wilusz, R.E., Zauscher, S., Guilak, F., 2013. Micromechanical mapping of early osteoarthritic changes in the pericellular matrix of human articular cartilage. Osteoarthr. Cartil. 21, 1895-1903.
- Yang, Q., Ma, Q., Herum, K.M., Wang, C., Patel, N., Lee, J., Wang, S., Yen, T.M., Wang, J., Tang, H., Lo, Y.H., Head, B.P., Azam, F., Xu, S., Cauwenberghs, G., McCulloch, A.D., John, S., Liu, Z., Lal, R., 2019. Array atomic force microscopy for real-time multiparametric analysis. Proc. Natl. Acad. Sci. U. S. A. 116, 5872-5877.

- Zelenski, N.A., Leddy, H.A., Sanchez-Adams, J., Zhang, J., Bonaldo, P., Liedtke, W., Guilak, F., 2015. Type VI collagen regulates pericellular matrix properties, chondrocyte swelling, and mechanotransduction in mouse articular cartilage. Arthritis Rheumatol. 67, 1286-1294.
- Zhou, S., Panse, K.S., Motevaselian, M.H., Aluru, N.R., Zhang, Y., 2020a. Three-dimensional molecular mapping of ionic liquids at electrified interfaces. ACS Nano 14, 17515-17523.
- Zhou, Y., Kastner, M.J., Tighe, T.B., Du, J., 2020b. Elastic modulus mapping for bovine cortical bone from submillimeter- to submicron-scales using PeakForce Tapping atomic force microscopy. Extreme Mech. Lett. 41, 101031.

# **Figures**

## Figure 1

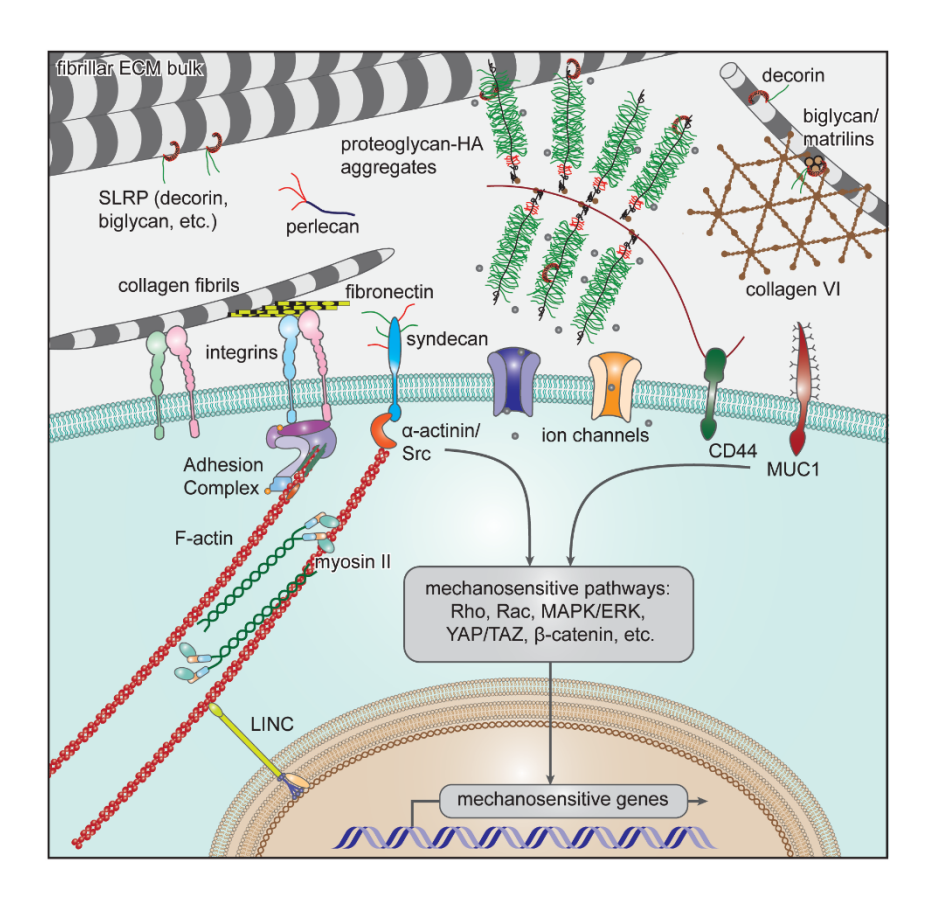


Figure 2

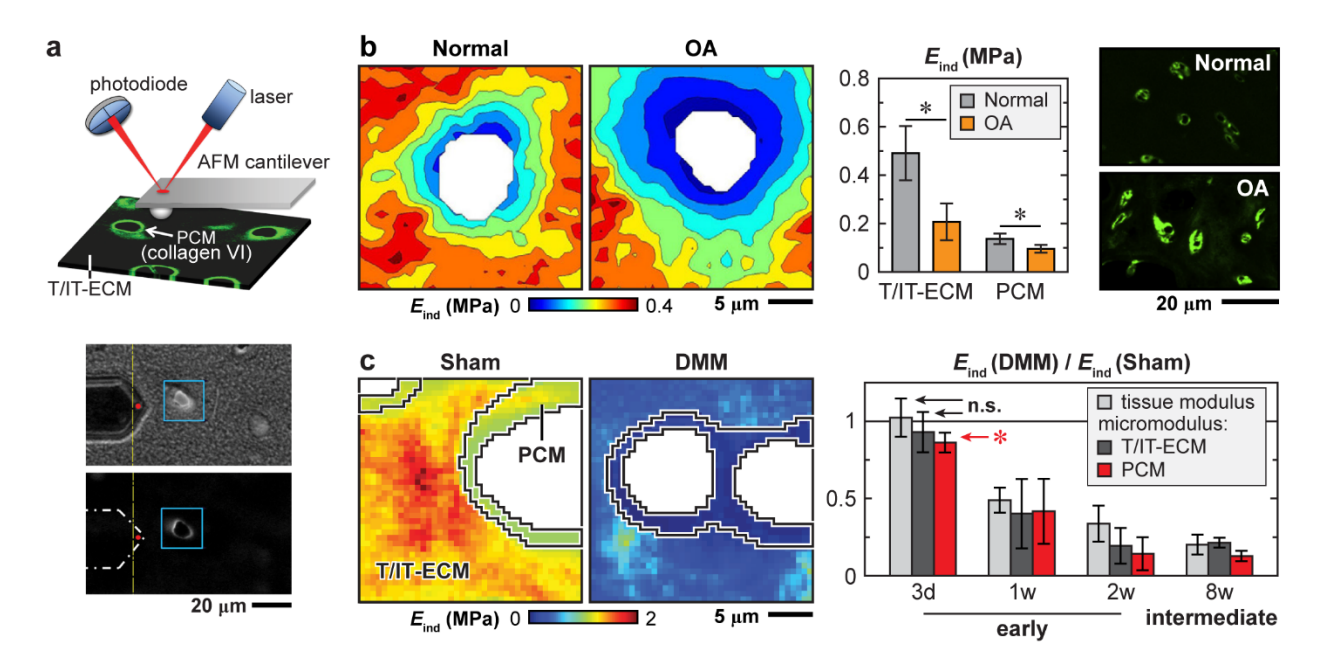


Figure 3

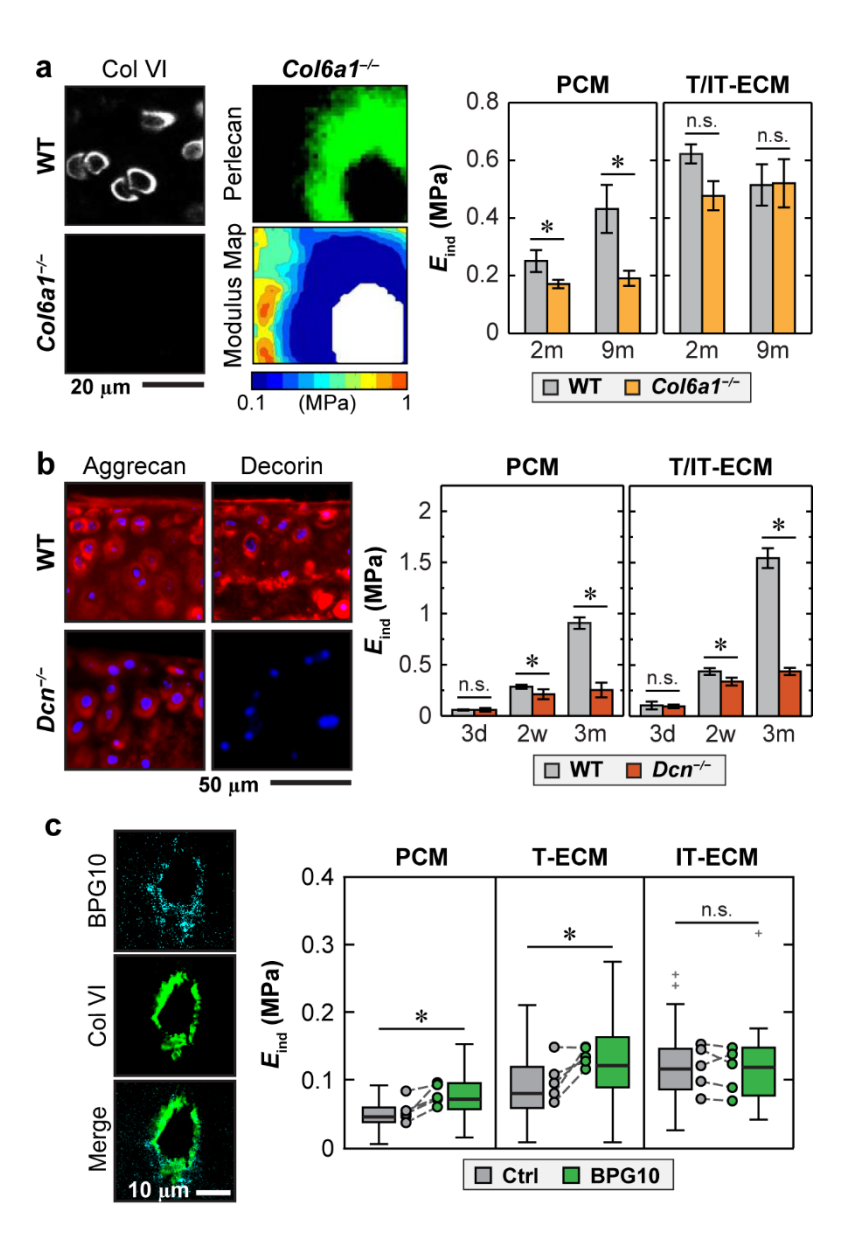


Figure 4

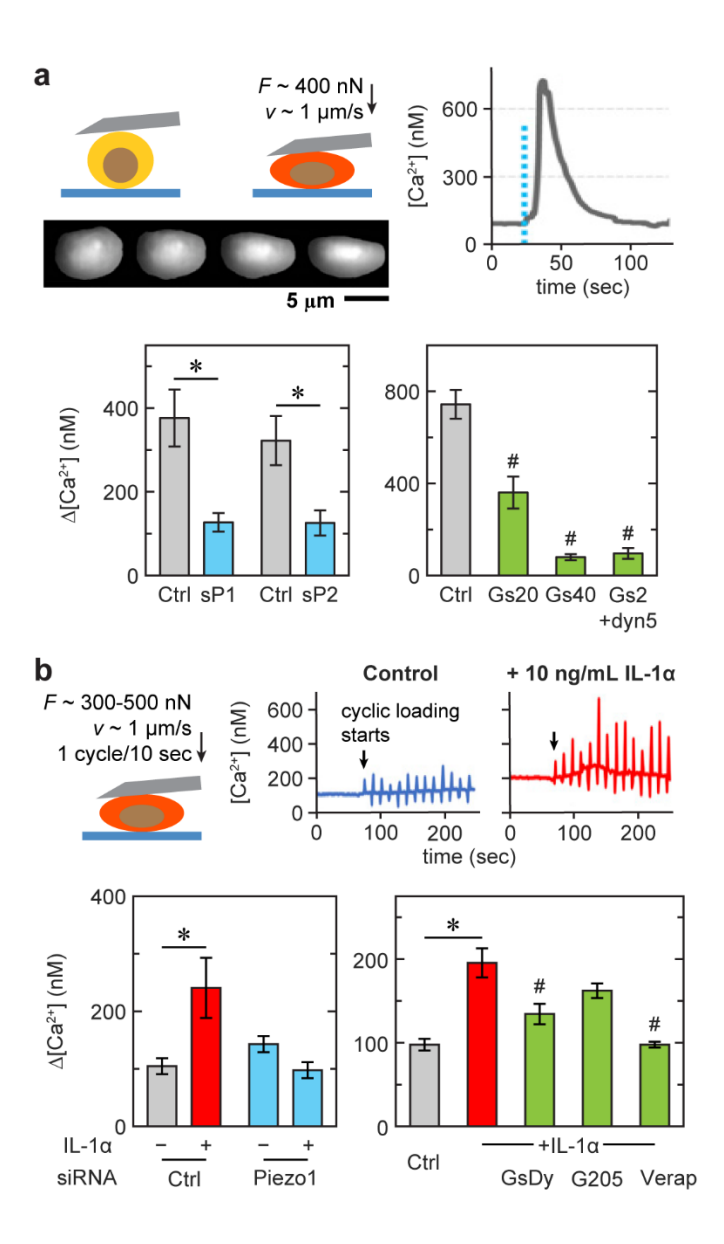


Figure 5

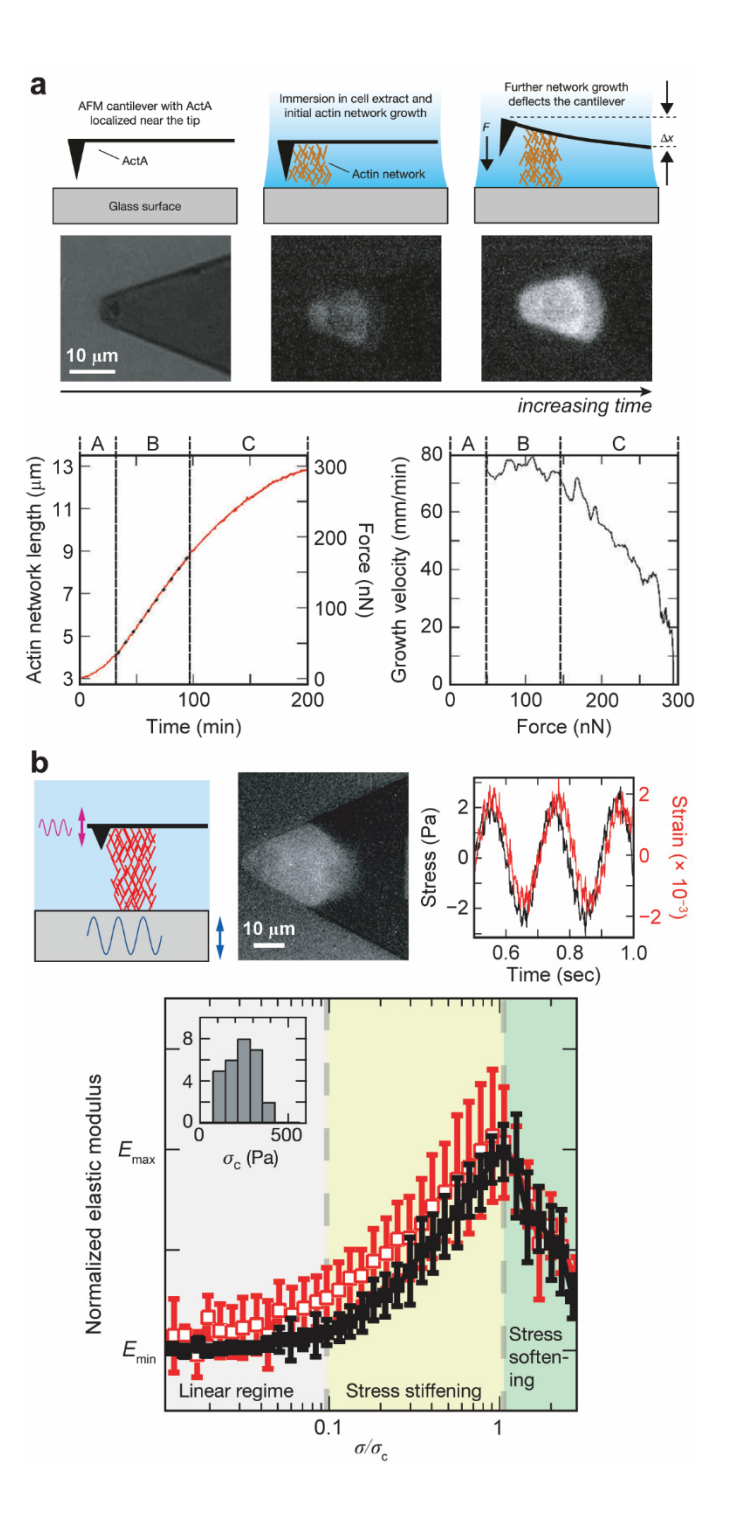
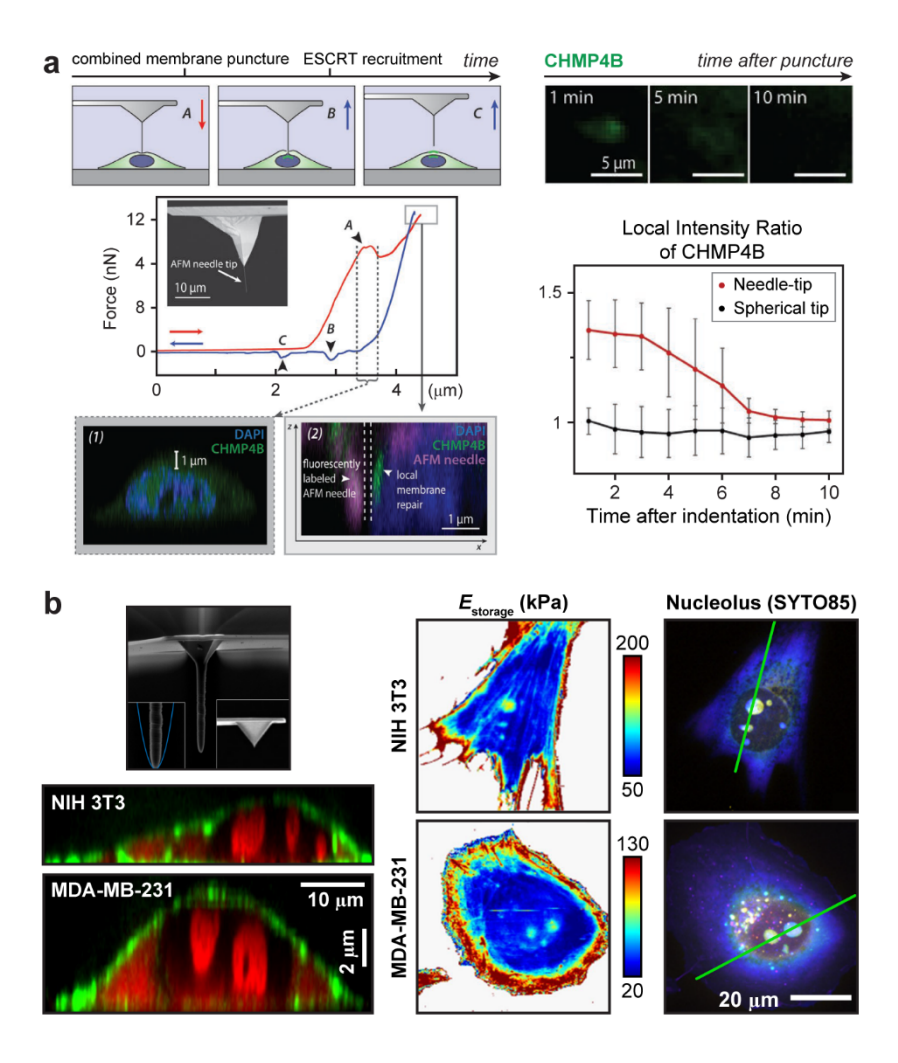


Figure 6



## Figure 7

